Novel boehmite transformation into γ-alumina and preparation of efficient nickel base alumina porous extrudates for plasma-assisted CO2 methanation

Federico Azzolina-Jury

Version of Record: https://www.sciencedirect.com/science/article/pii/S1226086X18309687
Manuscript_26c359d2f8c5a6db114fb18cbb772d2a

Novel boehmite transformation into γ-alumina and preparation of efficient nickel base alumina porous extrudates for plasma-assisted CO_2 methanation

Federico AZZOLINA-JURY

Normandie Université, ENSICAEN, UNICAEN, CNRS, Laboratoire Catalyse et Spectrochimie, 14000, Caen, France

***** Corresponding author: **federico.azzolina-jury@ensicaen.fr**

Abstract

Homogeneous low pressure cold plasma glow discharge was used for both boehmite to gamma alumina transformation as well as for catalytic CO_2 conversion into methane.

Novel plasma-assisted boehmite transformation into alumina was successfully achieved at lower temperature (80°C less) and shorter period of time (1 hour less) than the classical transformation. The final alumina structure properties were improved. The mechanism of the novel plasma-assisted boehmite transformation was addressed. Nickel alumina porous extrudate preparation was optimized and fully characterized. The amounts of binder and nitric acid used during the preparation of extrudates were studied. The concentration of nitric acid presented a major role in the catalytic properties of these catalysts leading to the improvement of the active phase dispersion and reducibility. As a result, methane yield was also improved with support acidity. A simulation study was performed in order to evaluate the influence of the extrudates dimensions on the pressure developed inside the reactor and on the glow discharge stability. It was demonstrated by simulation the need of shaping the nickel alumina catalysts for allowing the generation of a stable plasma discharge

through the catalytic bed. Plasma-assisted CO_2 hydrogenation under partial vacuum was carried out using the optimized nickel alumina extrudates. Formulation of efficient nickel alumina porous extrudates is provided for plasma or even industrial CO_2 methanation reactors.

Keywords: Plasma, CO_2 methanation, Nickel alumina extrudates, *operando* IR

1 Introduction

Carbon dioxide (CO_2) is a very stable molecule and a major responsible for the greenhouse effect. An interesting solution for reducing CO_2 emissions into the atmosphere is to use CO_2 as a chemical reactant to produce useful low-carbon fuels such as dimethyl ether, methanol and methane **[1]**. Methane (CH_4) has the higher heat of combustion among them. Besides, CH_4 does not need to be stored since it could directly be used after its production by injection into the already existing industrial natural gas pipelines. CO_2 can be also valorized and reduced into carbon monoxide (CO). In this case, CO-rich syngas produced from CO_2 hydrogenation can be used as reactant for Fischer-Tropsch reaction for manufacturing hydrocarbons and others valuable products such as aldehydes, alcohols, acids and ketones **[2-5]**.

CO_2 methanation using thermal heterogeneous catalysis has been widely studied in the last decades. Several metals have been used such as Rh, Ru, Pd, Ni, Co… **[6-10]** and also combined with various promoters such as Ce, La, W, Y … **[11-14]**. These metals have been supported on several materials such as Al_2O_3, SiO_2, zeolites and oxides **[1,15-19]**. Metallic nickel is an interesting active phase for this reaction since it presents an efficient catalytic activity and a low cost compared to the others metals. Alumina is an accurate candidate as

well for supporting metallic nickel because of its good stability, its relative high surface area and low cost.

Non-thermal plasma technology was found to be a potential solution for energy consumption reduction of catalytic processes. The synergy between the plasma and the catalyst from the possible effects of the plasma on the catalyst and of the catalyst on the plasma are excellently explained in literature **[20,21]**. Cold plasmas such as glow discharge, DBD… generate high amount of reactive species in the gas phase (ions and radicals). In some previous works **[1,22]** we reported the advantages of low pressure cold plasma in the case of CO_2 methanation. A major fact of cold plasma assistance is that CO_2 molecules can be firstly dissociated in the gas phase into CO at low temperature through electron impact and vibrational CO_2 excitation mechanisms **[1,22]** before reaching the catalyst surface. It is convenient to remind that in conventional catalysis; CO dissociation is the slowest reaction step and occurs over the catalyst surface at high temperatures. In a previous work **[1]**, we reported that plasma-assisted CO_2 hydrogenation under partial vacuum can be carried out at lower temperature (~100°C instead of 450°C) and residence time (700 times lower) with higher CO_2 conversion (65% at ~100°C against 45% at 450°C) and methane yield values (4% combining plasma and thermal catalysis at 300°C: synergy against 4% at 400°C under conventional heating) compared to conventional methods. Hence, higher CO_2 conversion and CO and CH_4 yields are obtained using cold plasma assistance.

Effective industrial utilization of porous catalysts requires a macroscopic shape of powder materials **[23]**. The shape of the catalysts should provide an accurate mechanical strength as well as a good resistance to attrition by keeping the same catalytic properties of the powders. Powder macroscopic shape will decrease the pressure drop inside the reactor as

well as the breakdown voltage needed to generate the glow discharge which is related to the energy efficiency of the plasma process. However, the pressure is not the only parameter that affects the breakdown voltage. It is well stablished in literature that other factors such as gas composition, size and morphology of the pellets, porosity of the catalytic bed and dielectric constant of the pellets play a crucial role in the low pressure glow-like discharge (this article) or atmospheric DBD plasmas generation. A decrease in pellet size, which is directly related to reducing bed porosity, leads to an increase in the breakdown voltage **[24]**. It has been proven by 2D axisymmetric DBD reactor modelling the importance of the contact points of the catalyst pellets (dielectric) where the plasma discharge is initiated because of the intensification of the electric field strength and the electron temperature **[25]**. The number of contact points can be increased by decreasing the porosity of the packed bed. Nevertheless, it has been proven that for low applied potential (this article) a high number of contact points will induce a Townsend discharge and the plasma will remain localized at the contact point regions. In order to spread the plasma out into the reactor bulk and to form a homogeneous glow-like discharge it is indispensable to increase the applied voltage or to consider the augmentation of the packed bed porosity through the adjustment of the pellets size. Moreover, local plasma discharges with high electron temperature can affect the catalytic adsorption processes affecting the useful surface area of the catalyst and deactivate the active sites by coke deposition in the case of reactions dealing with CO_2. The morphology of the packed bed particles is important as well. Pellet sharp edges enhance the electric field strength at the contact points **[26-29]** leading to high electron temperatures but lower electron density and reaction rates. Dielectric constant of the solid is another crucial factor to consider **[26,30]**. The electric

field is enhanced when the dielectric constant increases. In the presence of catalysts with high dielectric constant (i.e. ε $BaTiO_3$ = 4000) **[30]** the plasma will be localized and will not propagate through the packed bed **[26]** but the breakdown voltage will be lowered. In the case of low dielectric constant materials like gamma-alumina (ε γ-Al_2O_3 = 9-10) (this article) the breakdown voltage will be decreased when increasing the pellet size **[26]**. It is important to remind that the breakdown voltage is strongly dependent on the gas composition and this can been seen from the different Paschen curves well stablished in literature for different sorts of gases.

In the last years, plasma technology was shown to be also a promising technology for the preparation of efficient catalysts. Liu et al. **[31,32]** published interesting reviews about the use of cold and thermal plasmas in the preparation of materials. Plasma is used in three different cases: i) the synthesis of small size particle catalysts, ii) the deposition of the active phase on the support and iii) modification of catalysts. Many advantages of the use of plasmas in the preparation of catalysts are retained such as the improvement of their active phase (metal) dispersion, their catalytic activity and lifetime and reduction of their preparation time and associated energy requirements.

In the present work, homogeneous low pressure cold plasma (glow-like discharge) was used in: i) the boehmite transformation into γ-alumina and ii) the CO_2 methanation reaction in the presence of the efficient nickel base alumina porous extrudates.

The transformation of boehmite into transition alumina has been widely studied in the last decades **[33-36]**. The main interest of the dehydration of the aluminum oxihydroxide is the production of γ-alumina which is usually used as a catalyst support (this work) because of its high surface area and acidic properties. Glow-like plasma discharge allowed performing,

for the first time, the boehmite transformation into gamma alumina at lower temperature and shorter period of time than the conventional transformation. The final alumina powder presented higher surface area and lower pore size than the alumina obtained by classical boehmite transformation. The preparation of nickel alumina porous extrudates was optimized. A complete characterization study of the alumina extrudates was performed. The amounts of binder and nitric acid used during the preparation of extrudates were optimized. The concentration of nitric acid presented a major role in the catalytic properties (metal dispersion) of these extrudates. The low dielectric γ-Al_2O_3 pellets size and packed bed porosity were adjusted by controlling the pressure developed in the reactor in order to be able to generate a homogeneous glow-like discharge through the packed bed reactor under partial vacuum and low applied potential (2 kV peak-to-peak). A simulation study was performed in order to evaluate the influence of the extrudates dimensions on the pressure developed inside the reactor. Finally, homogeneous non-thermal glow discharge plasma was used for assisting the CO_2 hydrogenation reaction under partial vacuum using in-plasma (ICP) configuration **[1]** and the optimized nickel alumina extrudates.

2 Experimental

2.1 Transformation of boehmite into transition gamma alumina by plasma

Alumina powder was obtained from commercially available boehmite DISPAL 23N4-80 (Sasol) with large particles (50μm). Boehmite (AlOOH) was successfully transformed into gamma alumina after being irradiated by plasma under partial vacuum ($P < 5$ mbar) followed by thermal heating. The influence of the composition of the plasma (Pure O_2, Pure Ar and mixture of both), the irradiation time and the temperature of the thermal heating after plasma exposure were addressed. In the case of thermal heating, a molar mixture of

80% Ar and 20% O_2 was used. Boehmite powder was pressed ($1.96.10^5$ Pa) into self-supported wafers (2 cm^2, ~20 mg) for infrared measurements using the plasma *operando* IR-cell detailed in a previous work **[1]** (Figure 1B). In this cell, the wafer can be put in down position to be irradiated by the glow-like discharge plasma within the zone located between the two electrodes and in up position in which the wafer is surrounded by a heating jacket for thermal treatment. The plasma discharge is generated with a high voltage ac power supply (Resinblock transformer FART, 50 mA) with voltage and frequency of 2 kV and 50 Hz respectively. The top of the cell was connected to the gas system including mass flow controllers (Brooks). The boehmite transformation processes by plasma and by thermal heating were followed by *operando* infrared spectroscopy with a Bruker Vertex 80v FTIR spectrometer between 4000 and 1000 cm^{-1} (1 cm^{-1} optical resolution). The gases released during the transformation were identified by mass spectrometry using a Quadrupole Mass Spectrometer (Pfeiffer Omnistar GSD 301). The morphology and particles size were evaluated at different steps of the process by scanning electron microscopy. X-ray diffraction patterns were acquired during the transformation as well using a PANalytical X'Pert PRO diffractometer with CuKα radiation (λ = 0.15418 nm, 40 mA, 45 kV). The X-ray diffraction data of AlOOH and γ-Al_2O_3 powders were collected between 2Θ=5-75° at intervals of 0.1° with scan speed of 2° per min. The classical transformation of boehmite into gamma alumina was performed in order to have a reference. Thus, boehmite was calcined at 600°C during 2 hours with a heating rate of 3°C.min^{-1} in order to classically obtain the γ-Al_2O_3 form.

2.2 Nickel γ-Al_2O_3 porous extrudates preparation

It is important to point out that alumina extrudates can also be manufactured using other efficient kind of powder alumina such as synthesized nanosized γ-alumina **[37]**. Here, a binder was added to the plasma-treated γ-Al_2O_3 powder in order to prepare the alumina porous extrudates. The binder was obtained by peptisation of boehmite with nitric acid (HNO_3, 65%, Carlo Erba). No neutralization step with ammonia solution was used after the peptisation step in order to evaluate the influence of nitric acid on the rheological behavior of the alumina extrudate paste. The role of boehmite and nitric acid on the physicochemical properties of extrudates were addressed. The influence of the nitric acid (HNO_3/AlOOH molar ratio) was studied by keeping the same amount of boehmite and the influence of the boehmite amount was studied by keeping the same HNO_3/AlOOH molar ratio.

Before the kneading step, alumina powder, boehmite powder and nitric acid aqueous solution were mixed at room temperature to form a paste as indicated elsewhere **[38]**. The amount of water added to the acid solution was calculated in order to keep the same mass ratio of solids 'S' (boehmite + alumina powders) to liquids 'L' (nitric acid + water) **[38]**. Several extrudates were prepared with different amounts of nitric acid and boehmite by keeping the same S/L mass ratio equal to 1.3. Independently of the amounts of boehmite and acid, when the S/L mass ratio was lower than 1.3 the rheological properties of the paste were not accurate to be kneaded. Moreover, when the S/L mass ratio was higher than 1.3, the rheological properties of the paste were not acceptable because of the high amount of solids and the non-homogeneity of the paste. The alumina extrudates prepared for this study as well as for the catalytic tests are summarized in Table 1. To improve the understanding of the preparation of the different study cases, an example is given. For

example, for preparing the sample B30-A2 from 8 grams of gamma alumina powder, 30%, that is, 3.429 grams of boehmite are used. This amount corresponds to 0.057 moles of AlOOH. Now the HNO_3/AlOOH molar ratio of 1.95 should be applied to calculate the number of moles and mass (g) of nitric acid which are equal to 0.011 and 0.702 respectively. The weight of the aqueous nitric acid solution (65% wt.) can be estimated by dividing the nitric acid mass calculated previously by 0.65 giving 1.080 grams. The total amount of solids is the sum of boehmite and gamma alumina, that is, 11.430 grams. The total amount of liquid is now calculated from the S/L ratio of 1.3. The liquid represents 8.790 grams. The amount of water to add is estimated by subtracting the mass of the nitric acid aqueous solution to the total mass of liquids, that is, 8.790-1.080 = 7.710 grams. The acid concentration is finally obtained as the ratio between the number of acid moles and the volume of the liquid solutions which are obtained using the densities of the water and nitric acid aqueous solution at room temperature (1.00 and 1.21 $g.cm^{-3}$ respectively). In this example, the concentration of the nitric acid is 1.29 moles per liter.

Table 1: Al_2O_3 extrudates optimization study and Ni-Al_2O_3 extrudates for plasma-assisted CO_2 hydrogenation

	% AlOOH (wt.)	% HNO_3/AlOOH molar ratio	[HNO_3] ($mol.L^{-1}$)	% Nickel (wt.)	Code
Boehmite study	15	1.95	0.063	0	B15
	20	1.95	0.084	0	B20
	24	1.95	0.101	0	B24
	30	1.95	0.127	0	B30
	40	1.95	0.169	0	B40
	100	1.95	0.425	0	B100

Nitric acid study	30	1.95	0.127	0	B30-A2
	30	6.50	0.425	0	B30-A7
	30	19.50	1.295	0	B30-A20
Plasma-assisted CO_2 hydrogenation catalytic study	30	1.95	0.127	0	B30-A2
	30	1.95	0.127	15	B30-A2-N15
	30	6.50	0.425	15	B30-A7-N15
	30	19.50	1.295	15	B30-A20-N15

Cylindrical extrudates were made by extruding the paste through a cast of 3 mm diameter using Stainless Steel Makin's Professional extruder. Afterwards, extrudates were dried in an oven at 140°C during 1 h and then calcined in a muffle at 600°C with a heating rate of 3°C.min^{-1} during 2 h, as suggested elsewhere **[38]**.

The plasma CO_2 hydrogenation catalytic tests were performed under the same conditions (CO_2/H_2 molar ratio and total volumetric flow) than in a previous work **[1]** for catalysts activity comparison. Pressure reactor was simulated for different extrudates length. The smaller the extrudates dimensions the higher the reactor pressure is. A high pressure would enhance the selectivity towards methane since CO_2 methanation is a volume-reducing reaction. However, a low pressure would decrease the breakdown voltage and favor the energy efficiency of the plasma process. Besides, low pressure is convenient regarding the lifetime of species generated by the plasma discharge and the plasma stability. Extrudates were manufactured with 1 cm length and 3 mm diameter after simulation study. These dimensions allow having the same bed porosity as in a previous

work **[1]** (and same developed pressure inside the reactor) in order to compare their catalytic activity on CO_2 methanation under plasma at low pressure.

Nickel introduction (15% wt.) in alumina extrudates, prepared with different nitric acid amounts, was performed by wet impregnation using an aqueous solution of nickel nitrate hexahydrate ($Ni(NO_3)_2.6H_2O$, Merck > 99%) with a 0.1M concentration (Table 1). Water was then removed using a rotary-evaporator at 80°C under partial vacuum. Nickel doped alumina extrudates were then calcined at 450°C with a heating ramp of 2°C.min^{-1} during 4 h under static ambient air.

2.3 Characterization of Nickel γ-Al_2O_3 porous extrudates

The structure of nickel doped alumina extrudates was verified using a PANalytical X'Pert PRO diffractometer with CuKα radiation (λ = 0.15418 nm, 40 mA, 45 kV). The X-ray diffractrogrames were acquired between 2Θ = 5-75° at intervals of 0.1° with scan speed of 2° per min.

Nitrogen adsorption-desorption isotherms were measured at 77 K with a Micrometrics Model ASAP 2020 volumetric adsorption analyzer. Alumina extrudates were outgassed at 220°C overnight prior to analysis. The specific surface area of extrudates was determined from the Brunauer-Emmet-Teller (BET) equation. Their total pore volume (mesoporous volume) was estimated from the N_2 adsorbed volume at P/P_0 = 0.99.

The size and morphology of the binder (AlOOH) and of the alumina extrudates were examined with a Philips XL-30 scanning electron microscope (SEM) with acceleration voltage of 30 kV.

Temperature-programmed reduction (TPR) was performed on a Micromeritics AutoChem II analyzer to calculate the reducibility of the nickel phase supported on alumina extrudates.

Samples of 40 mg of nickel doped alumina extrudates were loaded inside a quartz U-tube. TPR was performed using a 5% v/v H_2 in Ar with a total gas flow of 40 mL.min^{-1} (STP) from room temperature to 1000°C and a heating ramp of 10°C.min^{-1}.

In situ FTIR measurements of the different alumina extrudates were performed with a NicoletMagna 550 FTIR spectrometer using 4 cm^{-1} optical resolution. Alumina extrudates were grinded and further pressed (1.96.10^5 Pa) into self-supported wafers (2 cm^2 and ~20 mg). Prior to infrared measurements, samples were activated under secondary vacuum at 450°C during 6 h with a heating ramp of 3°C.min^{-1}. Wafers were heated up to 500°C with the same heating ramp and reduced consecutively two times during 30 minutes with 100 Torr of H_2. Small volume doses of 1.57 mL containing the molecule probe (CO or C_5H_5N) were sent to the sample until complete saturation. Pyridine adsorption was carried out at 150°C to quantify the acidity of the catalysts and CO was adsorbed at room temperature to characterize the metal active phase of alumina extrudates. Lewis acidic sites quantification was estimated from pyridine adsorption by integrating the band at 1452 cm^{-1} once the adsorption equilibrium was reached and after desorption of physisorbed pyridine under secondary vacuum (1 x 10^{-6} Torr) at 150°C.

Computational fluid dynamics was performed in order to understand the dynamic behavior of the plasma reactor. Velocity and pressure profiles were simulated and analyzed with COMSOL Multiphysics® 5.3a for different extrudate dimensions.

2.4 Plasma-assisted catalytic CO_2 hydrogenation tests

The experimental set-up used for the plasma-assisted CO_2 hydrogenation reactions under partial vacuum is presented in Fig.1.

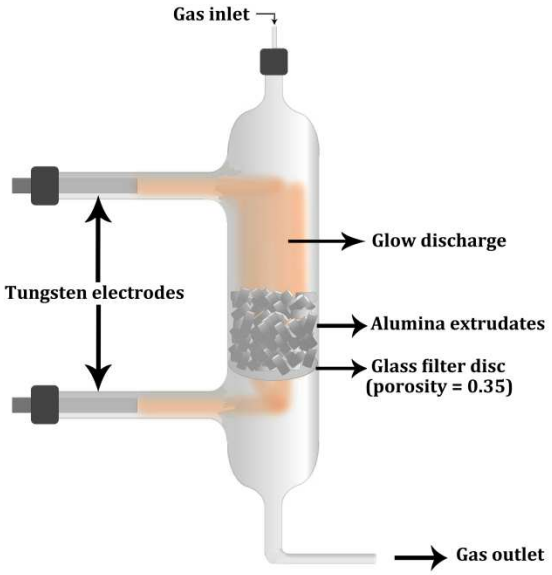

Figure 1: Packed bed plasma reactor for CO_2 hydrogenation under partial vacuum

The Pyrex ® glass plasma reactor (2 cm internal diameter) is made up of two tungsten electrodes separated by 13.5 cm. The glow discharge was generated with a high voltage AC power supply at 2 kV and 50 Hz. The catalytic tests were carried out using IPC configuration **[1]**. In IPC (in-plasma catalysis) configuration, the plasma discharge is generated through the catalyst bed. A heating jacket was placed around the plasma reactor walls in order to control the reactor temperature when necessary. A thermocouple located at the reactor wall was used for controlling and measuring the reactor wall temperature during the reaction. This reactor wall temperature was related to the catalyst bed temperature through a calibration performed before running the catalytic tests. Three grams of catalyst extrudates were loaded inside the reactor and supported by a porous glass frit (porosity of 0.35). The composition of the reactor outlet flow gas was analyzed by a Quadrupole Mass Spectrometer (Pfeiffer Omnistar GSD 301) and by FTIR spectroscopy with a Bruker Vertex 80v FTIR spectrometer. The IR spectra were acquired between 4000 and 1000 cm^{-1} (1 cm^{-1} optical resolution). Prior to reaction tests, catalyst extrudates were activated under

secondary vacuum (1 x 10^{-6} Torr) inside the plasma reactor at 450°C during 2 h with a heating rate of 3°C.min^{-1}. Afterwards, a reduction was performed using a 5% v/v H_2 in Ar with a total gas flow of 30 mL.min^{-1} (STP) from room temperature to 500°C and a heating ramp of 10°C.min^{-1}. The consumption of H_2 was followed by mass spectrometry and the reduction step was stopped when the H_2 consumption was no longer detectable. CO_2 hydrogenation was carried out with a CO_2/H_2 molar ratio of 1:4 and a total gas flow of 20 ml.min^{-1} (STP). Under these experimental conditions, the reaction was not internal/external diffusion-limited **[1]**. CO_2 conversion, CH_4 and CO selectivity and yields definitions are presented in Supplementary table 1. The flow rate of each reaction reactant and product was estimated from the total volumetric flow and from the MS and FTIR calibration curves, in which concentration of a given compound is plotted as a function of the MS and FTIR intensities.

Plasma-assisted CO_2 hydrogenation was studied without and with external heating in order to evaluate the effect of temperature coupled to plasma from 200°C to 400°C. Beyond 400°C plasma was not stable probably due to an increase in plasma current.

CO_2 hydrogenation was carried out under conventional heating for comparison purpose. The reaction was studied between 125°C and 450°C.

3 Results and discussions

3.1 Transformation of γ-AlOOH into γ-Al_2O_3 by plasma

The conventional dehydration of boehmite was studied by Frost et al. **[39]** by infrared spectroscopy. The boehmite transformation could be followed by the decrease in intensity of the hydroxyl stretching (3600-2900 cm^{-1}) and hydroxyl deformation modes (1050-900 cm^{-1}) with temperature. The asymmetric OH bending mode of AlO-H boehmite remained

constant with temperature up to 450°C. Beyond this temperature, this IR band intensity became equal to zero. However, the symmetric OH bending mode of AlO-H boehmite slightly decreased with temperature up to 450°C from which a large decrease in intensity was observed. The transformation process is usually achieved at high temperatures after several hours.

Here, boehmite was conventionally dehydrated to obtain γ-alumina (reference) by thermal heating at 600°C during 2 hours using a heating ramp of 3°C.min^{-1}. The XRD patterns (Fig 2a), the absorption FTIR spectra (Fig 2c) and SEM images of boehmite and gamma alumina (Fig 2b) are presented in Fig.2. The conventional transformation was verified by XRD. SEM images showed that boehmite particles of 10-40 μm were transformed into γ-alumina particles of 2-5 μm. The absorption FTIR spectrum of boehmite showed that water and CO_2 from the ambient were presented on the γ-AlOOH surface before the transformation. After boehmite dehydration, the γ-Al_2O_3 OH groups of type II (3729 cm^{-1}) and type III (3671 cm^{-1}) **[33-36]** were observed. CO_2 molecules were present on boehmite surface as hydrogencarbonates and as monodentate carbonates and were desorbed after thermal heating. Adsorbed water was also released after the thermal treatment. This fact was evidenced by the decrease of the broad OH band at high frequencies. The IR band assignments are summarized on Table 2.

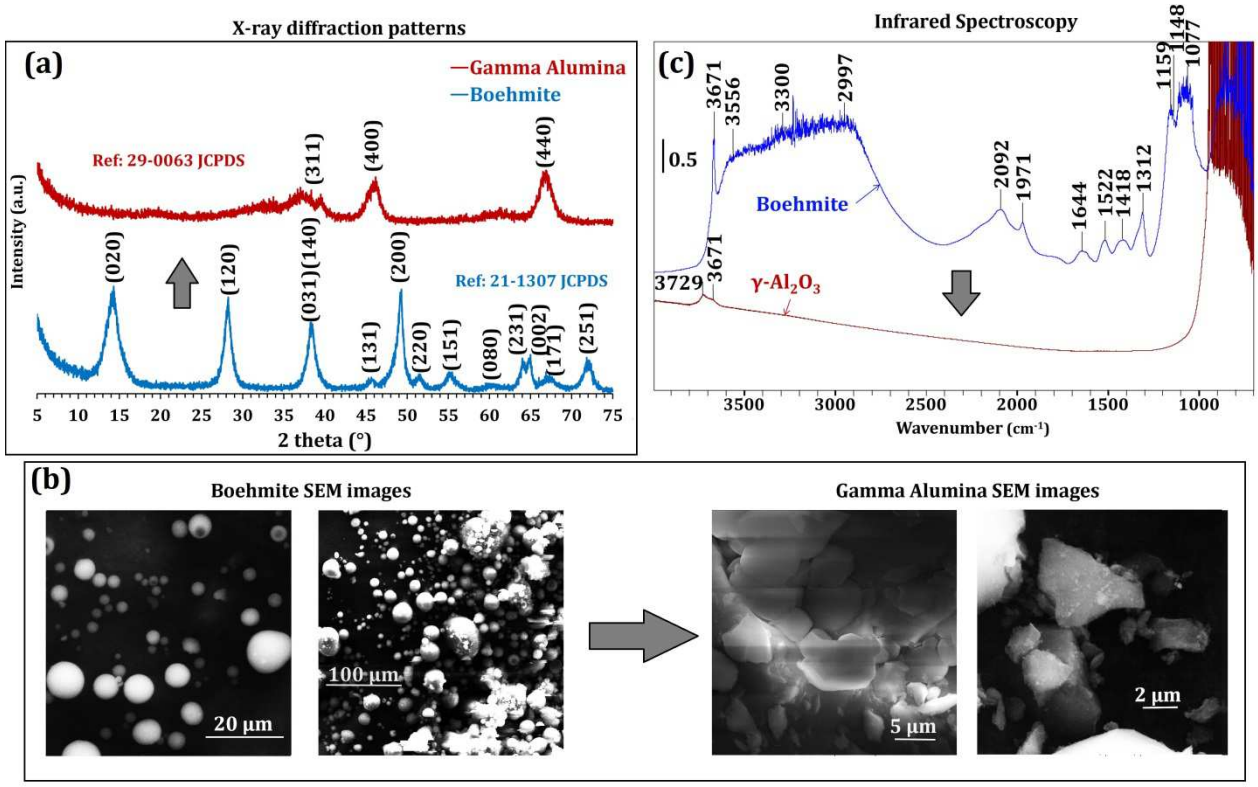

Figure 2: Characterization of conventional transformation of γ-AlOOH into γ-Al_2O_3 at 600°C for 2 h

Several gas mixtures of O_2 and Ar for plasma treatment were studied. It is important to point out that no significant differences on the final textural properties of gamma alumina were observed with respect to the plasma composition. However, the boehmite transformation mechanism was different. Hydrogen was release as a consequence of boehmite dehydroxylation process. Mass spectrometry hydrogen signal increased during plasma treatment (with pure O_2 or with pure Ar plasmas) as well as during the thermal treatment (Fig. 3a). In all cases, hydrogen was released as a consequence of the boehmite structure transformation. Hydrogen could not be produced by water splitting from water released in all cases. Under conventional heating, high temperatures (800-900°C) are needed to dissociate water into O_2 and H_2. Besides, the low energy glow discharge used in this study did not allow achieving water splitting. Moreover, from Figure 3a, the O_2 signal

was not increased during hydrogen release. This fact evidenced the absence of water splitting. During pure Ar plasma treatment, the highest hydrogen production was observed (116.07 cc H_2 STP) with the highest hydrogen release rate (10.2 cc H_2 STP/min) (Fig. 3a) compared to pure O_2 plasma or conventional treatment. During pure O_2 treatment, the hydrogen production and the hydrogen release rate were 3.36 times and 1.5 times lower respectively than in the case of pure Ar. However, when pure O_2 plasma was used, higher amount of water (free and adsorbed) was observed than in the case of pure Ar. During O_2 plasma treatment, oxygen was consumed (see Fig. 3a) since the oxygen radicals generated in the plasma produced water on the solid surface by combination with hydrogen coming from boehmite dehydroxylation. This fact is in agreement with the increase in intensity of the bands at 1618 and 1586 cm^{-1} (OH bending mode of adsorbed water) (Fig 3b). When pure Ar plasma was used MS O_2 signal was not altered. In the case of conventional boehmite treatment, hydrogen production was observed but only from 450°C. At this temperature, the hydrogen production was 1.8 times higher than in the case of 10 minutes pure O_2 plasma treatment but 1.8 times lower than in the case of 10 minutes pure Ar treatment. However, the hydrogen release rate was slow compared to those of plasma treatment (Fig 3a).

FTIR *operando* was applied to boehmite transformation under pure oxygen plasma during 10 minutes (Fig 3b). After this period of time, no more changes were observed in the IR spectra's band intensities. CO_2 molecules adsorbed on the surface were desorbed. Hydrogencarbonates were completely desorbed since the intensity of the IR bands at 3556, 1644, 1418 and 1148 cm^{-1} disappeared after 10 minutes. The more stable monodentate carbonates species were partially desorbed. The IR bands at 1522 and 1312 cm^{-1} were

decreased and red-shifted. This latter fact indicated a diminution of these species on the alumina surface.

Table 2: IR bands assignment

	Species	Mode	Band position (cm^{-1})	Reference
Adsorbed species	Hydrogencarbonates	νOH stretch	3556	**[40-42]**
		ν_{as}OCO stretch	1644	
		ν_{s}OCO stretch	1418	
		δOH bend	1148	
	Monodentate carbonates	ν_{as}OCO stretch	1522	**[42]**
		ν_{s}OCO stretch	1312	
γ-AlOOH	AlO-H stretching vibration of AlO-H (boehmite) (ν_1)		3671	
	Asym. Deformation vibration of AlO-H (boehmite)		1159	**[39,42,43]**
	AlO-H stretching vibration of AlO-H (boehmite) (ν_2)		3300	**[39,43-45]**
	Asym. stretching vibration of AlO-H (boehmite) (ν_3)		2997	
	Sym. Stretching vibration of AlO-H (boehmite) (ν_4)		2092	
	Combination vibration of AlO-H (boehmite)		1971	
	Sym. Deformation vibration of AlO-H (boehmite)		1077	**[39,43,46,47]**
γ-Al_2O_3	Hydroxyl groups	νOH stretch	3729	**[33-36,42]**
			3671	

The transformation of γ-AlOOH into γ-Al_2O_3 was started after plasma ignition and evidenced by the intensity decrease in boehmite hydroxyl stretching and bending modes. The IR bands at 3671, 3300, 2997 and 2092 cm^{-1} ascribed to AlO-H stretching modes of

boehmite hydroxyls were diminished with irradiation time. The IR bands at 1159 and 1077 cm^{-1} attributed to AlO-H deformation modes of boehmite hydroxyls decreased as well. It was observed by mass spectrometry that the amount of hydrogen released was higher when plasma treatment was applied than in the case of classical heating indicating a more efficient dehydroxylation by plasma.

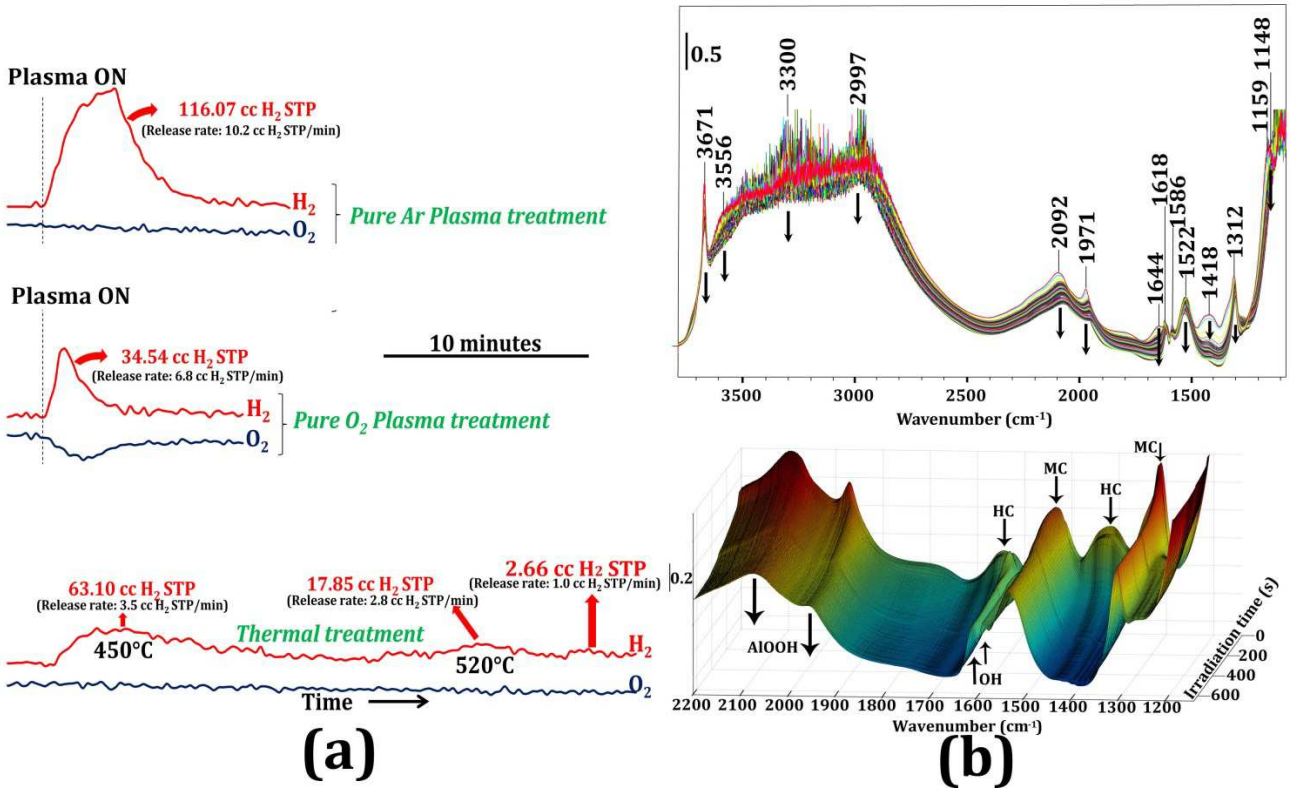

Figure 3: Mass spectrometry signal of H_2 (red) and O_2 (blue) during plasma and thermal treatment of boehmite (a); *Operando* analysis of plasma treatment on boehmite (b)

The incomplete boehmite dehydration by plasma could be explained by the fact that plasma rather interacts with the surface of boehmite, that is, the bulk of the material since it might not be formed inside the material pores. It is very important then to determine if plasma was generated inside the material pores during the boehmite transformation in order to establish the real active surface reached and treated by plasma. Discharges could be formed inside the material pores by electron impact ionization within the pore **[48]**. Zhang et al.

studied the influence of the material dielectric constant (from 4 to 1000) and pore size (μm) on the possibility of plasma generation inside the pores. They concluded that the probability of plasma discharge inside the material pores is enhanced for low dielectric constant materials such as Al_2O_3 (this article) and even for small pore sizes (μm). However, it is unlikely that plasma was generated inside the pores of the material during boehmite transformation because the pore sizes in this study are more than three orders of magnitude smaller than those studied in **[48]**. Moreover, sidewall effects mentioned in **[48]** would be more important in nanosized pores (this article). In other work of Zhang et al. **[49]** it has been claimed that plasma generation within the material pores is only possible for pores sizes in the micrometer range. Plasma can only be generated inside the material pores during boehmite transformation if the Debye length is lower than the average material pore diameter. In this work, a potential of 2kV and 50 Hz were applied with a relatively high electron density ($\simeq 10^{17}$ m^{-3}) and electron temperature $T_e \simeq 3$ eV (34800 K). If the ion temperature (T_i) is neglected with respect to T_e, Debye length can be estimated by:

$$\lambda_D = \sqrt{\frac{\varepsilon_0 \times k_B \times T_e}{n \times e^2}} \qquad \textbf{Eq. 1}$$

where λ_D is the Debye length, ε_0 is the permittivity of free space (8.85×10^{-12} $F.m^{-1}$), k_B is the Boltzmann constant (1.38×10^{-23} $J.K^{-1}$), e is the charge of an electron ($1.6 \times 10_{-19}$ C), T_e is the temperature of the electrons (K), n is the density of electrons (m^{-3}).

The Debye length is equal to $\simeq$ 41 μm which is three orders of magnitude larger than this study material pore size and plasma cannot be formed inside the material pores. Excited and ionized species generated within the plasma discharge could diffuse inside the material

pores. However, the mean free path of these species will be significantly small as a consequence of the small material pore size. Thus, the lifetime of these active species will be considerably reduced and no changes within the material pores can be induced.

Therefore, plasma superficial treatment was not enough to induce a complete dehydration of boehmite into gamma alumina but significant changes were observed under plasma irradiation in the first 10 minutes. In Figure 4 left, XRD patterns of the boehmite treated with different plasma composition are presented.

In order to complete the transformation process, thermal heating was applied after plasma treatment. The transformation of boehmite treated by plasma was analyzed by XRD, FTIR *operando* spectroscopy and SEM. Different temperatures of the post-thermal treatment were studied as a function of time (Fig.4). It is important to point out that no significant differences were observed with respect to the plasma composition in terms of XRD patterns, powder morphology (SEM) or surface area. In order to simplify data, characterization of boehmite powders treated with pure O_2 plasma followed by conventional heating is shown only. After 10 minutes of plasma irradiation, XRD patterns shown that boehmite phases were still present. SEM images evidenced the presence of boehmite spherical particles as well. Transformation was partially achieved when thermal heating was applied at 450°C during 45 minutes. Nevertheless, the dehydroxylation was only completed when the temperature of the thermal treatment was 520°C. The transformation process during the post-thermal treatment was followed by FTIR *operando* spectroscopy (Fig.5).

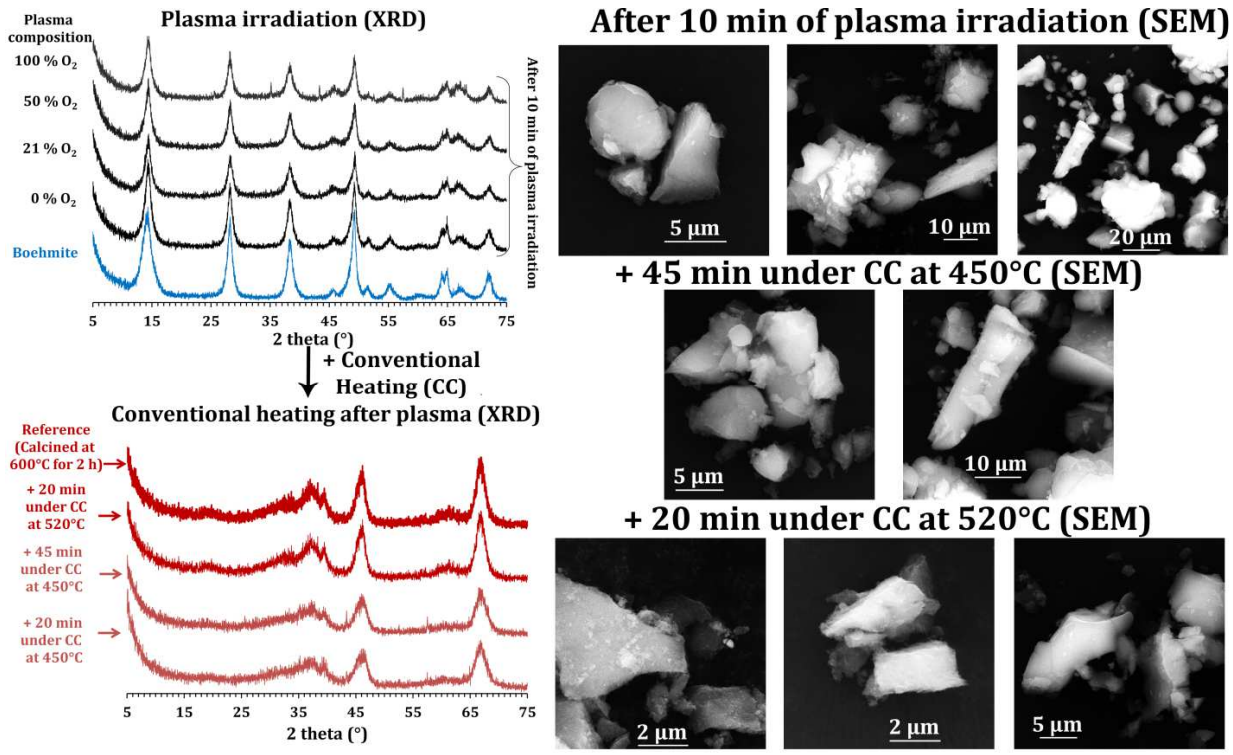

Figure 4: Thermal post-treatment study after plasma irradiation for successfully transform γ-AlOOH into γ-Al_2O_3

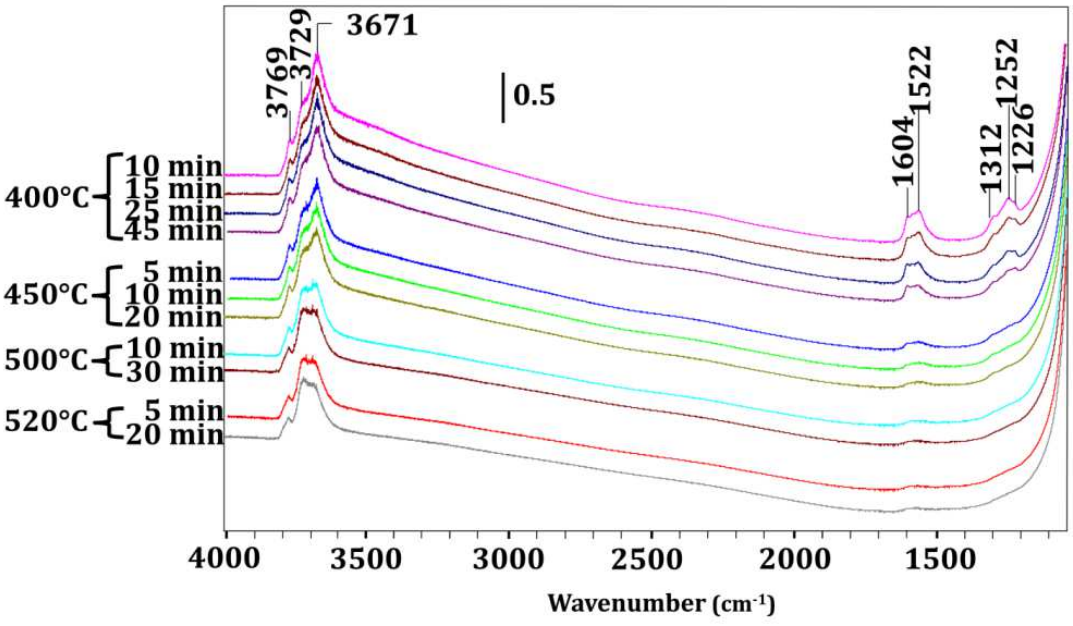

Figure 5: FTIR *operando* analysis of post-thermal treatment at different temperatures

FTIR *operando* analysis of post-thermal treatment at 400°C revealed a new band at 3769 cm^{-1} which was not possible to observe when the transformation process was carried out

completely under conventional heating at 600°C during 2 h. Carbonates were still remaining on the surface at 400°C (1522 and 1312 cm^{-1}). The bands at 1604, 1252 and 1226 cm^{-1} could be ascribed to hydrogen-bonded OH groups. At 520°C the transformation process was achieved. OH groups at 3729 and 3671 cm^{-1} were observed as in the case of the boehmite calcined at 600°C during 2 h (reference). According to literature **[50-52]**, these bands are associated with a type II_6 OH group and with a type III OH group respectively. A new type I_6 OH group at 3769 cm^{-1} was observed when plasma treatment was applied. This fact could indicate that high energetic species generated in the plasma might interact with different γ-AlOOH facets compared to conventional dehydration. The IR bands at 3729 and 3671 cm^{-1} are more intense (50% more) when plasma treatment was applied than in the case of thermal heating. This fact could be due to the differences found in terms of hydrogen and water release in both processes.

The surface area, the pore volume and the pore size of the γ-Al_2O_3 obtained with and without plasma treatment are presented in Table 3.

Table 3: Characterization of γ-alumina treated with and without plasma

γ-Al_2O_3	Surface area (m^2/g)	Mesoporous volume (cm^3/g)	Pore size (nm)
With plasma	261	0.37	5.43
Without plasma	155	0.44	11.44

Plasma treatment allowed obtaining a higher surface area γ-alumina (+70%) with smaller pore size (-50%) and lower pore volume (-15%) with respect to the conventional alumina (without plasma treatment). The amount of water released in the case of combination of pure O_2 plasma and conventional heating for boehmite transformation was lower than in the case of thermal boehmite transformation. In the first case, 2.6 cc H_2O STP were released

while in the second case, the water release was equal to 3.7 cc H_2O STP. The different hydrogen and water release in both cases could explain the differences observed in terms of the final structural gamma alumina properties. The boehmite transformation mechanism involves two main steps: i) structural collapse of AlOOH after hydrogen transfers and water release and ii) Al migration for building the final γ-Al_2O_3 structure **[53]**. In addition, γ-Al_2O_3 is a relatively high dielectric constant material (this work) that has a high capacity of trapping charges (high-energy electrons) as a quasi-stationary electron film at the material surface with a lifetime up to several days **[54-56]**. It is possible that the charged material particles are stabilized by electrons trapped at the surface. Thus, particles agglomeration during plasma-assisted boehmite transformation could be minimized and the final γ-Al_2O_3 textural properties are then improved.

The whole transformation process could be achieved in a shorter period of time and at lower temperature (520°C) when plasma treatment was applied. Dehydroxylation rate of boehmite was higher under plasma assistance than during classical transformation (Fig. 3).

3.2 Optimization of nickel γ-Al_2O_3 porous extrudates formulation

The amounts of nitric acid and boehmite (binder) were studied. These amounts were optimized based on the extrudate yield defined as the ratio between the final and the initial mass of solids weighed before and after extrudate preparation.

The binder amount was varied from 15 to 100%. The maximum extrudate yield (around 75%) was obtained using an optimum amount of boehmite (binder) of 30% (Fig.6). Afterwards, the HNO_3/AlOOH molar ratio using 30% of binder was varied from 1.95 to 19.50%. The increase of the nitric acid amount during the extrudate preparation raised the alumina extrudate paste viscosity and lowered the extrudate yield as shown in Fig.6. The

optimum HNO_3/AlOOH molar ratio, in terms of alumina extrudate yield, was 1.95% without any neutralization step during the preparation of the extrudate paste. However, the extrudate yield could be easily improved using ammonia solution after the peptisation step.

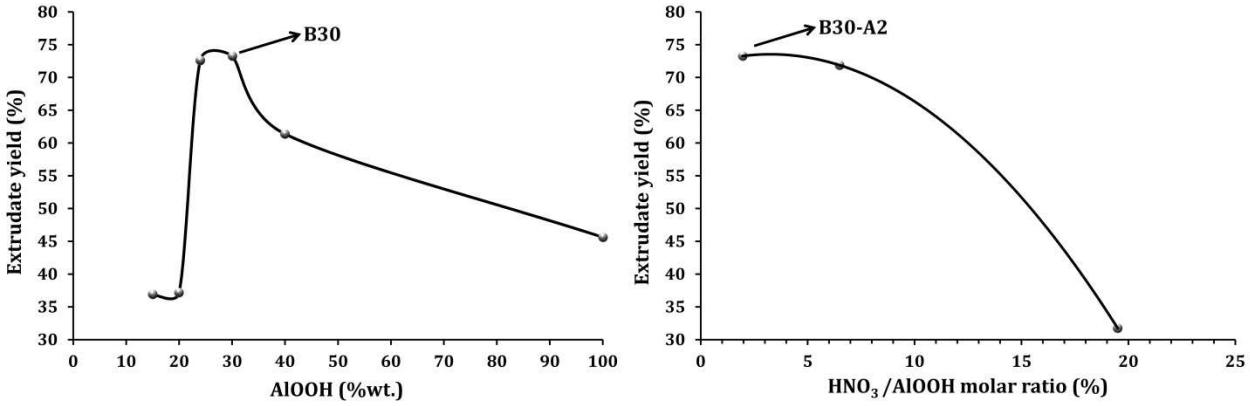

Figure 6: Optimization of alumina porous extrudates preparation

The surface area, the pore volume and the pore size of the different γ-Al_2O_3 porous extrudates are summarized in Table 4. The pore sizes were determined by BET method on the adsorption branch of the isotherms. The amount of acid and binder did not produce significant changes in the specific surface area, pore volume and pore size of the different alumina porous extrudates.

Table 4: Characterization of γ-alumina porous extrudates

Alumina extrudate code	Surface area (m^2/g)	Mesoporous volume (cm^3/g)	Pore size (nm)
B15	145	0.44	12.3
B20	147	0.44	12.1
B24	145	0.44	11.4
B30	147	0.44	12.1
B40	148	0.44	12.0
B100	148	0.42	11.4

B30-A2	149	0.44	11.9
B30-A7	147	0.44	12.0
B30-A20	145	0.43	12.0
B30-A2-N15	123	0.33	10.7
B30-A7-N15	120	0.33	11.0
B30-A20-N15	118	0.32	10.9

Wafers of 20 mg were made to evaluate the nitric acid amount influence on the total acidity of the alumina support extrudates. The pyridine adsorption spectra can be found in supplementary Figure S1. Brønsted acid sites were not observed through the formation of pyridinium ions at 1545 cm^{-1}. Lewis acid sites, which were the only responsible of the total acidity of alumina samples, were identified by the band at 1452 cm^{-1}. These sites were verified by the presence of the bands at 1613 and 1625 cm^{-1} ascribed to medium strong and strong Lewis acid sites respectively **[33]**. Lewis acid sites could be generated during the high-temperature dehydroxylation in the final alumina extrudates preparation step. The different types of OH groups were disturbed during pyridine adsorption and bands between 3250 and 2900 cm^{-1} assigned to combinations and harmonics of the aromatic cycle bands increased as well (Fig. S1). Lewis and Brønsted acidic sites were quantify using the extinction coefficients reported in the literature: $\varepsilon(pyL)=2.22$ $cm.\mu mol^{-1}$ for Lewis sites and $\varepsilon(pyH^{+})= 1.3$ $cm.\mu mol^{-1}$ for Brønsted sites **[34,57]**. The surfaces of the wafers (cm^2) were carefully measured using *Image J* software. The area of the bands (cm^{-1}) at 1545 and 1452 cm^{-1} were evaluated after heating the samples at 150°C in order to eliminate physisorbed pyridine. These bands areas were then multiplied by the surface of the wafers and divided

by their mass (g). The area at 1545 cm^{-1} was zero for all cases indicating that Brønsted sites are not present. The acid sites quantification is summarized in Table 5. The experimental acidity error was 5%.

Table 5: Acidity quantification of alumina extrudates prepared with different amount of nitric acid

Alumina extrudate code	Lewis acid sites [μmol/g]	Total acid sites [μmol/g]
B30-A2	147.13	147.13
B30-A7	211.66	211.66
B30-A20	215.06	215.06
B30-A2-N15	122.06	122.06
B30-A7-N15	139.34	139.34
B30-A20-N15	146.56	146.56

Nitric acid showed to play a role in the number of acid sites. The B30-A20 support catalyst as well as the B30-A20-N15 catalyst presented the highest acidity.

Nickel was introduced by wet impregnation in the alumina supports B30-A2, B30-A7 and B30-A20 to study the influence of the HNO_3 amount used in the preparation of alumina extrudates on the metal reducibility and metal species distribution over the support. Ni-alumina wafers of 20 mg were used for *in situ* CO and pyridine adsorption experiments. Prior to analysis, wafers were reduced two times at 500°C under 100 Torr of H_2 during 30 minutes. The surface area, pore volume and size of alumina extrudates were diminished after nickel loading for the three cases by 18%, 25% and 10% respectively (Table 4). As a consequence, Lewis acidity of the three catalysts was also diminished after nickel

introduction by 17% in the case of B30-A2 and by 30% in the case of B30-A7 and B30-A20 (Table 5).

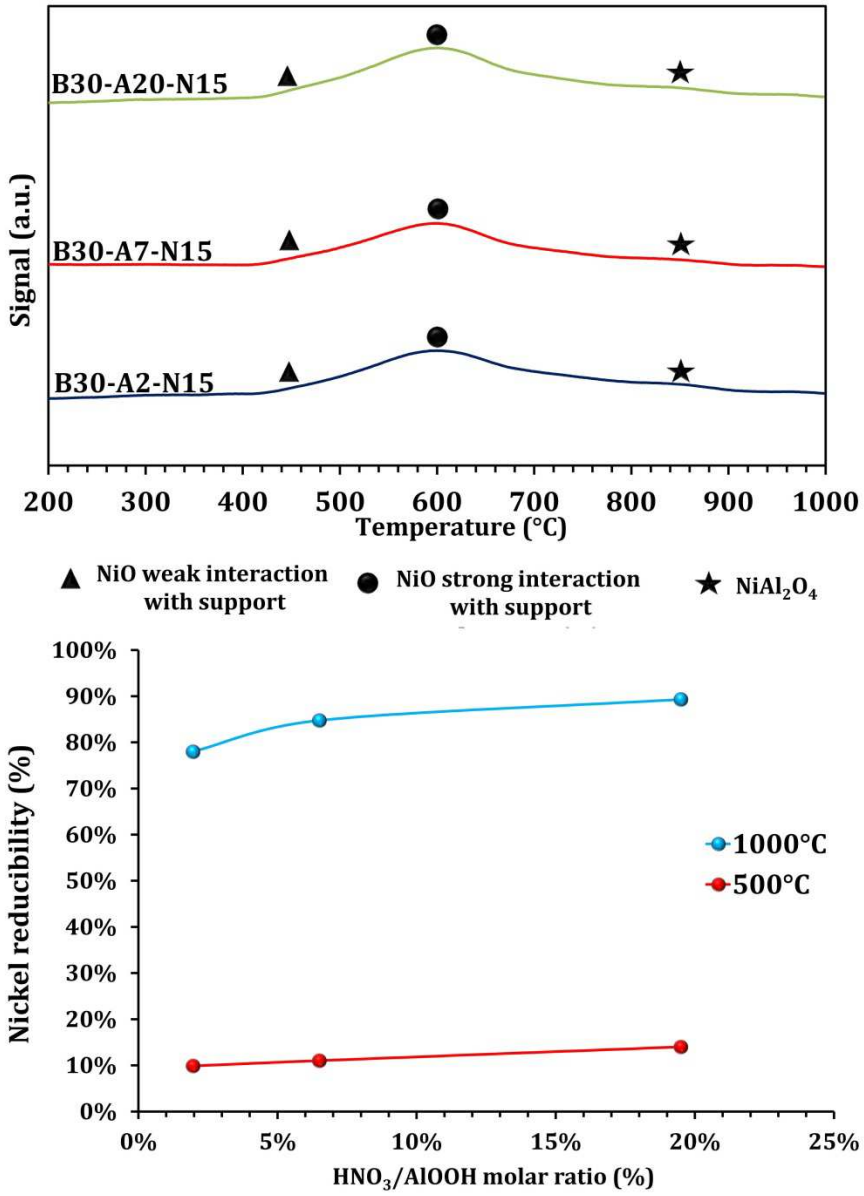

Figure 7: Influence of the HNO_3 amount on the nickel species and reducibility

The calcination was performed at 450°C after metal introduction in order to avoid the formation of $NiAl_2O_4$ spinel species which are difficult to reduce and inactive for CO_2 methanation **[58]**.

H_2-TPR profiles showed several nickel species: H_2 consumption started at 450°C attributed to NiO species with weak interaction with the alumina support and a peak at 600°C assigned to NiO species with strong interaction with the support. No peak was observed at around 850°C indicating the absence of $NiAl_2O_4$ spinel species (Fig. 7) **[59,60]**. The position of spinel species at 850°C is pointed in Figure 7 to indicate their absence. The reducibility of nickel was calculated as the molar ratio between the amount of reduced nickel and the total amount of nickel introduced to the sample. The experimental error was found to be equal to 2%. The amount of HNO_3 used in the alumina extrudate preparation improved the nickel reducibility at both 500 and 1000°C (Fig. 7). For example, at 500°C, the increase of HNO_3/AlOOH from 1.95% to 6.50% enhanced the reducibility in 12% and from 1.95% to 19.50% in 42%.

CO adsorption spectra of samples B30-A2-N15, B30-A7-N15 and B30-A20-N15 are shown in Fig.8.

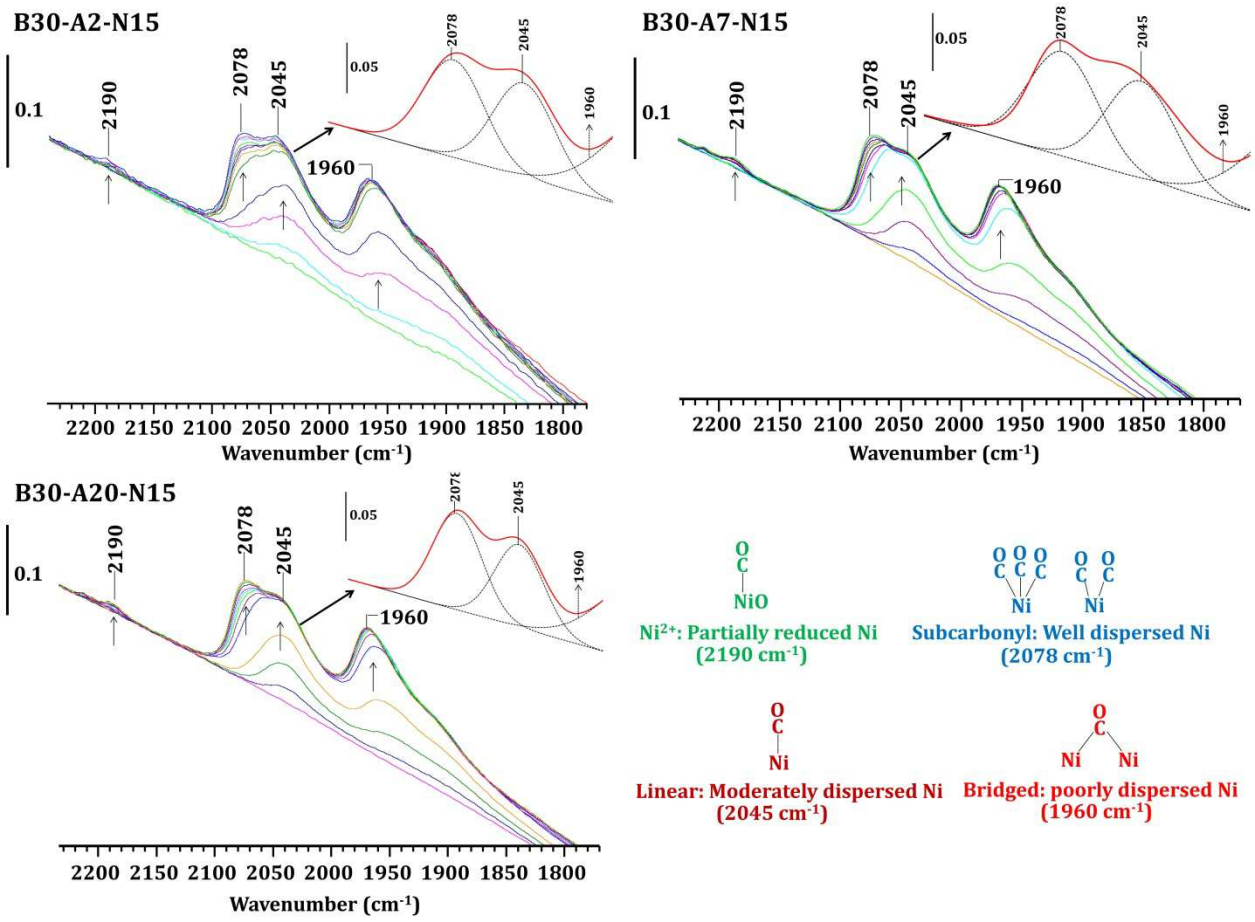

Figure 8: Study of nickel dispersion by *in situ* FTIR CO adsorption

Small doses of CO were adsorbed on nickel alumina wafers until full coverage of the metal. Four IR bands were observed: i) at 2190 cm^{-1} ascribed to partially reduced nickel; ii) at 2078 cm^{-1} assigned to subcarbonyls species which evidence a well dispersed Ni; iii) at 2045 cm^{-1} attributed to linear carbonyls showing moderately dispersed Ni and iv) at 1960 cm^{-1} assigned to bridged carbonyls indicating the presence of poorly dispersed Ni **[61]**. The four bands were blue-shifted with CO adsorption until reaching saturation. At full CO coverage of the active phase, the areas of the different bands were calculated using exactly the same integration limits and baseline. The experimental area error was estimated to be 2%. A deconvolution was applied to estimate the areas of the bands at 2078 and 2045 cm^{-1}.

Table 6: Active phase characterization by CO adsorption

Alumina extrudate code	Partially reduced Ni	Well dispersed Ni	Moderately dispersed Ni	Poorly dispersed Ni	L/B ratio	Adsorbed CO at full coverage (μmolCo/g)
	Area (cm^{-1})	Area (cm^{-1})	Area (cm^{-1})	Area (cm^{-1})		
B30-A2-N15	0.09	2.41	2.33	5.30	0.44	264
B30-A7-N15	0.10	2.53	2.37	4.54	0.52	266
B30-A20-N15	0.14	2.89	2.49	4.03	0.62	275

The dispersion of the metal was favored with the amount of HNO_3 used during the preparation of alumina extrudates (Table 6). The amount (areas) of well and moderately dispersed metallic nickel increased and poorly dispersed nickel decreased with HNO_3 concentration. The linear to bridge (L/B) adsorbed CO with nitric acid concentration. The nickel particle size usually is decreased when the L/B ratio is increased **[62]**. This fact could explain why the partially reduced Ni increased with the L/B ratio and with the acid nitric concentration. The increase of the acid concentration during the alumina extrudate preparation favored the metal dispersion. Besides, the catalyst resistance to coke formation could be enhanced **[62]**. Since an improvement of the metal dispersion is related to a decrease in metal particle size, the Ni particle sizes of the three cases were estimated using Scherrer equation using the XRD patterns for two different angles: 43.5° and 63.1° (Fig. S2). The particle nickel size of the samples B30-A20-N15, B30-A7-N15 and B30-A2-N15 were estimated to be 7, 10 and 11 nm respectively for the two Bragg angles. This fact indicates that the increase of the acid concentration during the alumina extrudate preparation lowered the metallic nickel particle size. Efficient nickel base alumina extrudates could be

prepared using 30% wt. of binder and 19.50% HNO_3/AlOOH molar ratio. A neutralization step with ammonia solution should be used after the peptisation step in order to enhance the extrudate yield (Fig. 6).

3.3 Simulation study

The pressure inside the reactor was estimated by simulation using COMSOL Multiphysics 5.3a for different extrudate lengths. This pressure was compared to the critical pressure at which the applied voltage is equal to the breakdown voltage. Pressure inside the reactor should be lower than the critical pressure in order to be able to generate a stable glow discharge between the electrodes across the catalytic bed.

A first estimation of the critical pressure for the three gases used for CO_2 methanation reaction at the reactor inlet (Ar, H_2, CO_2), was performed using the Paschen law. Since the electrodes distance (13.5 cm) was considerably higher than the electrodes radii (0.6 cm), a correction factor for scaling Paschen law was applied **[63]**. Additionally, this correction considers the modification of gas breakdown voltages by plasma-wall interactions. The critical pressures for the three gases were calculated for 2 kV (applied voltage). In case of argon, secondary Townsend coefficient of 0.095 **[64]** was adopted for classical Paschen law and a factor 'b' of 0.131 **[63]** for the Scaling law. The values of p.d for CO_2, Ar (scaling law), Ar and H_2 were 22.5, 54.7, 66.1 and 78.1 respectively (Fig.S3). The critical pressure estimated for CO_2, Ar (scaling law), Ar and H_2 were 227.7, 553.6, 669.0 and 790.5 Pa respectively.

In plasma packed bed reactors, the catalytic bed reduces the breakdown voltage depending on the nature of the catalyst, the particle size and the shape of particles **[65]** that might create localized electric field strengths and even change the discharge nature **[66]**. The

presence of the catalytic bed should shift the Paschen curves giving a higher value of critical pressure for a given breakdown voltage and electrode distance. In order to prove this point, the plasma reactor was loaded with 3 g of Ni-Al_2O_3 extrudate catalyst. The extrudates length was 1 cm and the porosity of the bed (φ) was calculated using equation 2 (ρ_{bed}: density of the bed and ρ_{ext}: density of the extrudates) and was found to be 0.42. The extrudates density was firstly estimated by measuring the mass and volume of several extrudates (50) and the average extrudate density was found to be 1.46 $g.cm^{-3}$.

$$\boldsymbol{\varphi = 1 - \frac{\rho_{bed}}{\rho_{ext}}} \qquad \textbf{Eq.2}$$

The reaction flow rates used for CO_2 methanation were set (10 mL/min STP Ar; 8 mL/min STP H_2; 2 mL/min STP CO_2) and the pressure inside the reactor was increased by closing a valve located at the reactor outlet. The glow discharge became unstable at 15 Torr (1974 Pa) and the plasma was not able to be generated when pressure was higher than 70 Torr (9210 Pa). Several simulations were run in order to estimate the influence of the extrudates length (bed porosity and permeability) on the pressure inside the reactor. Before carrying out this study, the permeability of the packed bed support (ROBU filter disc series 5, with porosity equal to 0.35) was estimated. Pressure was experimentally measured before and after the support disc at different flow rates (from 5 to 15 mL/min STP). COMSOL Multiphysics simulations were carried out in order to find the right value of the support permeability that matched the experimental pressures for each flow rate. Pressure and velocity profiles of these simulations are shown in supplementary files (S4-S8).

The permeability of the support slightly decreased with flow rate (Fig.9a). The experimental values were fitted (R^2 = 0.998) and the permeability for the reaction flow rate (20 mL/min STP) was found to be $4.480.10^{-11}$ m^2.

The extrudates length was varied from 0.8 to 3 cm. The sphericity of extrudates (ψ) was determined as the ratio of the surface area of equivalent-volume sphere to that of the actual extrudate particle using equation 3 **[67-69]**:

$$\boldsymbol{\psi = \frac{A_{sp}}{A_p} = \frac{\pi^{\frac{1}{3}}(6V_p)^{\frac{2}{3}}}{A_p}} \qquad \textbf{Eq.3}$$

where V_p is the volume of one non-spherical extrudate, A_p is the surface area of the cylindrical extrudate and A_{sp} is the surface area of the equivalent-volume sphere.

The volume-surface mean diameter (D_{vs}) was calculated after equation 4 **[69]**:

$$\boldsymbol{D_{vs} = \frac{6V_p}{A_p\psi}} \qquad \textbf{Eq. 4}$$

Sauter mean diameter (D_{sd}), which is defined as the diameter of a sphere that has the same ratio of volume to surface area as the particle of interest, was calculated using equation 5 **[69]**:

$$\boldsymbol{D_{sd} = \frac{6V_p}{A_p} = \psi D_{vs}} \qquad \textbf{Eq. 5}$$

The introduction of an effective diameter (D_{eff}) of cylindrical extrudates, which is defined as the product of Sauter mean diameter and the extrudates sphericity, was proposed by Liangxing et al. **[69]** for more accurate estimation of pressure drop with non-spherical particles:

$$\boldsymbol{D_{eff} = \psi D_{sd}} \qquad \textbf{Eq. 6}$$

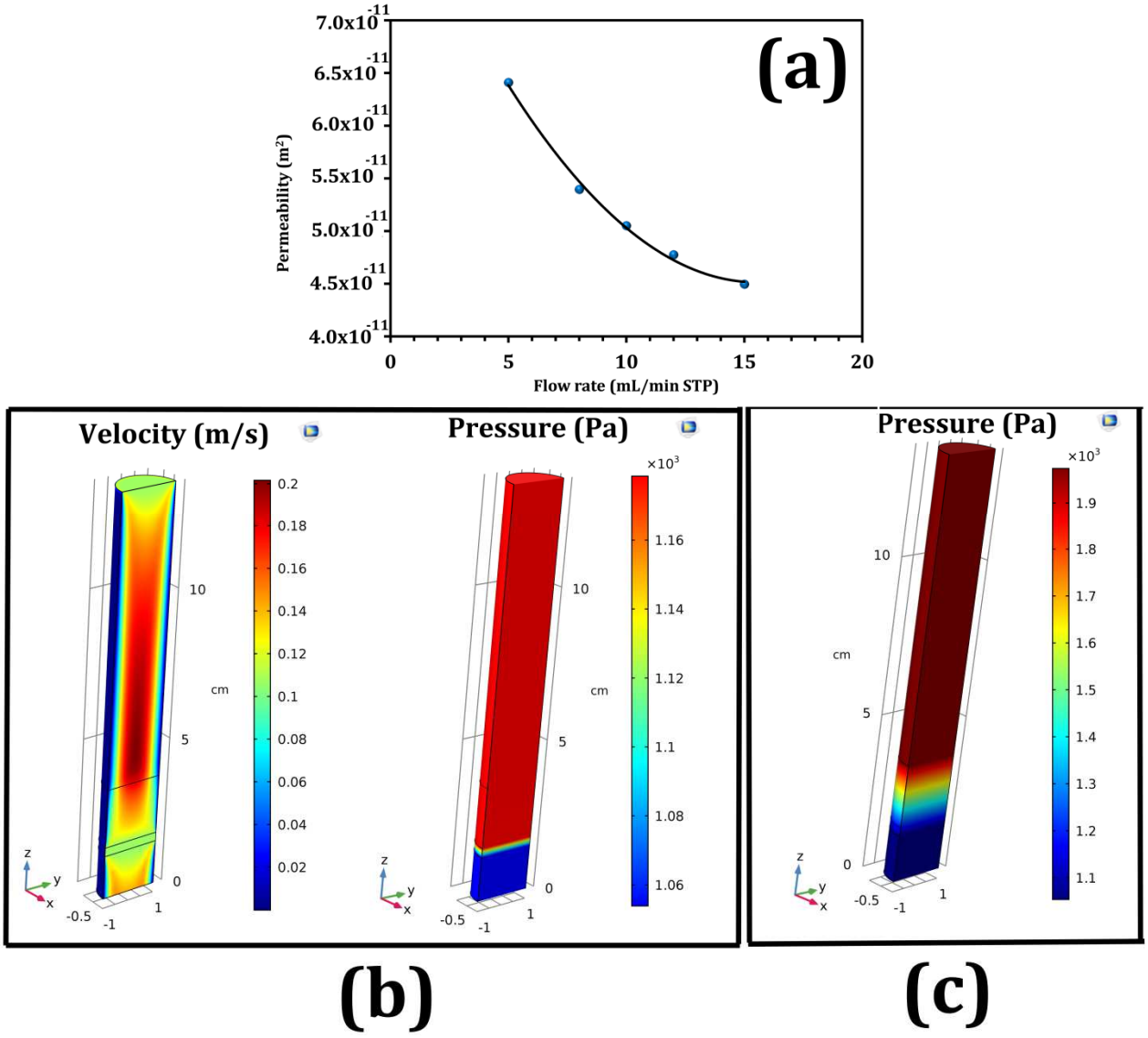

Figure 9: Disc permeability (a); velocity-pressure profile of plasma reactor (b); Pressure profile for critical extrudates dimensions (c)

The permeability of the catalytic bed was estimated using the Kozeny-Carman equation:

$$\boldsymbol{k = \frac{D_{eff}^2 \varphi^3}{K(1-\varphi)^2}} \qquad \textbf{Eq.7}$$

where K is a constant equal to 5 for packed bed reactors **[70]** and k (m^2) the permeability of the bed. The more accurate bed porosity for the different extrudates length was estimated using the empirical equation 8:

$$\varphi = \frac{A}{(D/d)^n} + B \qquad \textbf{Eq.8}$$

with A = 0.9198, B = 0.3414 and n = 2 for cylinders bed particles **[71]**. The simulations experiments are summarized in Table 7. Velocity and pressure profiles for the case of 1 cm cylindrical extrudate length are shown in Fig. 9b.

Table 7: Computational simulation of pressure inside the plasma reactor for different extrudates lengths

P_2 (Pa)	L (cm)	r (cm)	ψ	D_{eff} (cm)	φ	Bed permeability (m^2) (x 10^{-7})	P_1 (Pa) (simulated)
1053.95	0.80	0.30	0.80	0.30	0.362	2.13	1179.30
1053.95	0.90	0.30	0.78	0.30	0.362	2.11	1179.30
1053.95	1.00	0.30	0.76	0.30	0.362	2.07	1179.30
1053.95	1.50	0.30	0.70	0.28	0.360	1.85	1179.40
1053.95	2.00	0.30	0.65	0.27	0.358	1.64	1179.40
1053.95	2.50	0.30	0.61	0.26	0.357	1.47	1179.50
1053.95	3.00	0.30	0.58	0.25	0.356	1.33	1179.50

P_1: Pressure inside the reactor, P_2: Pressure at the reactor outlet, L: cylindrical extrudate length, r: cylindrical extrudate radii, ψ: sphericity, D_{eff}: effective diameter, φ: bed porosity.

The pressure generated inside the reactor remained lower than the pressure for which the glow discharge is instable (1974 Pa) for the whole cylindrical extrudate length range under study. The extrudate length influence on reactor pressure was found to be negligible. Pressure drop was mainly caused through the disc catalyst support. Simulations were run in order to estimate the critical extrudates dimensions for which the pressure inside the reactor becomes equal to 1974 Pa. The critical cylindrical extrudates length and radii were

found to be 57.8 and 28.9 μm respectively (Fig. 9c). This fact indicates that powder catalysts with low particle size (See section 2.1) are not possible to be used in the plasma reactor and that macroscopic shape of Ni-alumina catalysts is needed. Nickel alumina extrudates of 3 cm length were adopted for catalytic tests.

3.4 Plasma-assisted CO_2 hydrogenation

CO_2 hydrogenation was carried out under plasma assistance and conventional heating using the Ni-Al_2O_3 extrudates with different metal dispersion and reducibility. The CO_2 conversion, methane selectivity and methane and CO yields are shown in Fig. 10. The experimental relative error was estimated at 2% (error bars are not shown in the figure for clarity improvement). The error was estimated after three catalytic runs using fresh catalyst. All catalytic parameters were calculated after reaching a steady state for each temperature. CH_4, CO and H_2O were formed from CO_2 hydrogenation under partial vacuum.

CO_2 conversion was higher under plasma (40-50%) than under conventional heating (0-30%) for all temperatures. In an excellent review on plasma-assisted catalytic conversion of gaseous carbon dioxide and methane into valuable chemicals and fuels **[72]**, CO_2 conversions under different sorts of plasma and activation molecules were reported. CO_2 conversion activated with H_2 under surface discharge was 15% **[73]** and when CO_2 was activated with water under a negative corona discharge, CO_2 conversion was 18% **[74]**. DBD was used also for CO_2 activation with methane with different gaps from 1.8 to 1 mm and CO_2 conversion was found to be 20%**[75]**, 37%**[75]** and 43.1%**[76]** respectively. In this study, CO_2 conversion under a glow-like discharge was higher and equal to 40-50%.

Under plasma assistance, CO_2 conversion was higher with support only (without metal) than with nickel. The introduction of metals decreases the complex permittivity (dielectric

constant) of the catalyst **[77]**. The higher the complex permittivity, the lower the breakdown voltage was due to local electric field enhancement. Therefore, higher plasma energy was available to induce CO_2 dissociation into CO by electron impact and vibrational excitation of ground state CO_2 molecules **[1]**.

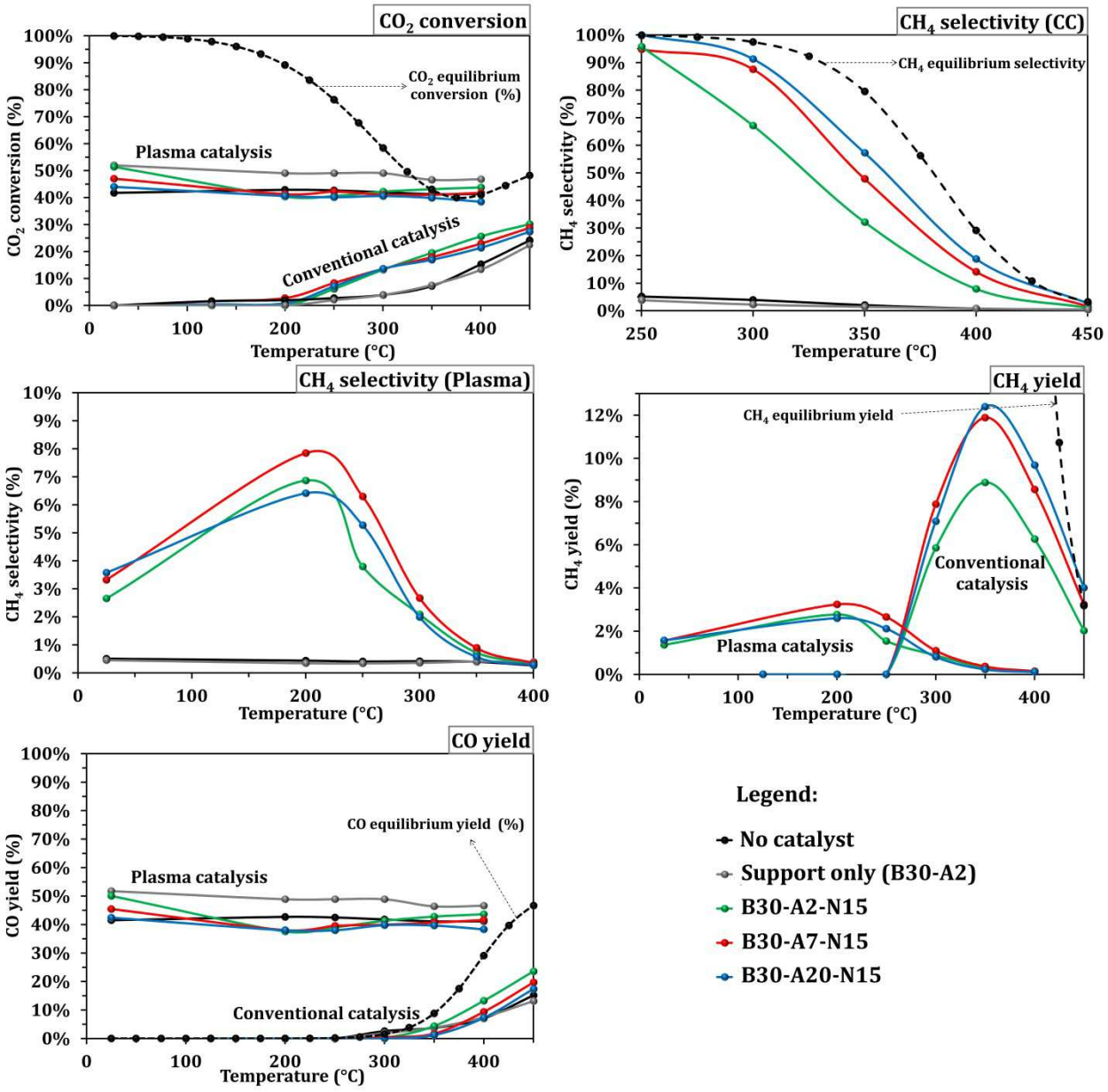

Figure 10: CO_2 conversion, CH_4 selectivity and yield of CO_2 hydrogenation under plasma and conventional heating

Under classical catalysis, catalysts were only active from 200°C and CO_2 conversion was favored with temperature. No significant differences were observed between the three Ni-

based catalysts. However, they presented a higher CO_2 conversion than in the case of the reaction carried out with support only and without any catalyst. In fact, metallic nickel offered adsorption sites for CO_2 molecules as monodentate formates before being dissociated into CO **[22]**.

Under conventional heating, methane selectivity was considerably improved following the trend: B30-A20-N15 > B30-A7-N15 > B30-A2-N15 in agreement with the previous characterization section. Negligible amounts of CH_4 were observed with support only and without any catalyst. CH_4 selectivity decreased (and CO selectivity increased) with temperature because of the exothermal character of the methanation reaction. Under plasma assistance, methane selectivity reached its maximum at 200°C. Nevertheless, no conclusions can be made since the differences observed for the three Ni-based catalysts are in the same order of magnitude than the experimental error (2%).

Under plasma assistance, a methane release was observed (not shown here) after plasma extinction as in a previous work **[1]**. CH_4 yield was between 2 and 4% with a maximum centered at 200°C. When methane release was not considered, CH_4 yield under plasma was lower than under conventional heating. This fact could be explained by partial CH_4 oxidation by plasma for syngas production. CH_4 yield decreased with temperature because of the CH_4 selectivity diminution.

Under conventional catalysis, higher temperature was needed to reach the maximum CH_4 yield. Under plasma, CO yield at low temperature was higher (~50%) than CO yield obtained through conventional catalysis at 450°C (~30%). CO_2 conversion was 40-50% under plasma at low temperature (near room temperature) and CO_2 conversion was only 30% under conventional catalysis at 450°C. The plasma catalysis process was more energy

efficient than the conventional one. In fact, two cartridges heaters of 200 W each were needed to maintain the temperature of the reactor at 450°C. It represented 400 W of power consumption. Under plasma, 2 kV and 20 mA were applied to generate the glow-like plasma discharge. It represented only 40 W. As a conclusion, the power consumed during plasma catalysis was roughly 10 times lower than in the case of conventional catalysis. Plus, CO_2 conversion, CO yield and CH_4 yield (only if methane release after plasma extinction is considered) were higher than in the case of conventional catalysis at lower temperature. It is important to point out that CO yield at low temperature produced by CO_2 splitting by plasma was significantly higher than that reported recently in literature under conventional catalysis using Cu supported on Al_2O_3 **[78]**.

Nitric acid concentration remarkably improved CH_4 yield because of the nickel dispersion and reducibility enhancement without the addition of a second expensive metal such as Ce. Moreover, CH_4 yield was found to be improved compare to Ni-USY catalysts used in a previous work under the same reaction conditions **[1]**.

4 Conclusions

Plasma-assisted transformation of boehmite (γ-AlOOH) into gamma alumina (γ-Al_2O_3) was addressed. Oxygen glow discharge plasma induced structure modifications on boehmite during the first 10 minutes of irradiation. Plasma treatment considerably increased the surface area of final γ-Al_2O_3 powder due to the lower temperature used in the transformation process compared to conventional dehydration. Pore size and volume decreased under plasma irradiation. Plasma was coupled to thermal heating and boehmite transformation was successfully achieved at lower temperature and period of time than in the classical transformation process. The mechanism of this transformation, with and

without plasma, was found to be different. This fact was evidenced by the higher hydrogen release rate during the boehmite irradiation and by the observation of new OH groups (type II_6) indicating that is possible that plasma induced changes on different γ-AlOOH facets.

Ni-Al_2O_3 porous extrudate manufacture was optimized. The amounts of binder and nitric acid were studied. The maximum extrudate yield was 75% for 30% of optimal binder concentration (B30). The extrudate yield decreased with nitric acid amount and neutralization step was needed for relatively high acid concentrations. No differences in terms of surface area, pore size and volume were observed for the range of binder and nitric acid concentration under study. The increase of the nitric acid concentration (HNO_3/AlOOH molar ratio) during extrudates preparation enhanced the acidity (Lewis) of the support (γ-Al_2O_3) and, as a consequence, the nickel reducibility and the nickel dispersion (as a function of the area associated to well dispersed nickel species). When the HNO_3/AlOOH molar ratio was increased from 1.95 to 19.50, the acidity of the support, the reducibility of the nickel (at 500°C) and its dispersion were improved in 46%, 42% and 20% respectively. Besides, nickel particle size was found to decrease with HNO_3 concentration and support acidity. When the HNO_3/AlOOH molar ratio was increased from 1.95 to 19.50%, the particle size was reduced in 35%. This is a major result concerning the improvement of the catalyst activity and catalyst resistance to coke formation.

A simulation study was carried out in order to optimize the extrudate dimensions. The critical pressure for which the glow discharge becomes unstable was experimentally measured and found to be equal to 1974 Pa. The 3 mm diameter extrudate length did not show any influence on the reactor pressure. The critical extrudate dimensions were estimated by simulations: 57.8 μm length and 28.9 μm radii. Simulation study proved that

Ni-Alumina extrudate catalysts must be macroscopic shaped and that powder catalysts cannot be used in the plasma reactor of this study.

CO_2 hydrogenation was performed under plasma assistance and thermal heating. CO_2 conversion was higher under plasma than under thermal heating for all the temperature range under study.

Under conventional heating, methane yield and selectivity were remarkably enhanced by HNO_3 concentration related to the enhancement of the metal dispersion and reducibility (B30-A20-N15 > B30-A7-N15 > B30-A2-N15).

The maximum of methane yield was observed at lower temperature and it was higher under plasma assistance (if the methane release after plasma extinction is considered) than in the case of conventional heating. CO yield was higher (~50%) under plasma assistance at low temperature (near room temperature) than in the case of conventional catalysis (~30%) at 450°C. The energy consumed during the plasma catalysis was roughly estimated to be 10 times lower than in the case of conventional catalysis.

More efficient low cost catalyst was prepared in this study in terms of methane yield compared to those prepared in a previous work **[1]**. In that case, Ni-USY zeolites used for the same reaction under identical reaction conditions shown a CH_4 yield of 4% (0.19 $mLCH_4$ STP/min.gNi) at 400°C under conventional heating and 2% (0.09 $mLCH_4$ STP/min.gNi) at 200°C under plasma assistance. In this work, Ni-alumina extrudates presented a CH_4 yield of 12.5% (0.55 $mLCH_4$ STP/min.gNi) at 350°C under conventional heating and 3.24% (0.14 $mLCH_4$ STP/min.gNi) at 200°C under plasma assistance. The catalysts prepared in this study presented a CH_4 yield 3 times higher under classical heating (at 350°C) and 1.5 times higher under plasma (at 200°C) than Ni-USY zeolites of the previous work **[1]**. This put in

evidence the importance of the remarkable results of this work concerning the preparation and optimization of low cost nickel supports for CO_2 methanation. CH_4 production could still be enhanced by using the optimized nickel alumina extrudates in an atmospheric pressure DBD plasma reactor or in an industrial packed bed reactor at atmospheric pressure. The optimized catalysts (nickel alumina porous extrudates) are currently being tested in a CO_2 methanation pilot plant at atmospheric pressure. The catalytic activity of these catalysts is remarkably stable after one continuous week of methanation test. CH_4 selectivity was found to be 100% and CH_4 yield was enhanced compared to the results available in literature (for thermal catalysis only). These catalysts will be used in an industrial CO_2 methanation unit. The optimized catalysts will be tested also in an atmospheric DBD plasma reactor for CO_2 methanation at laboratory scale.

ACKNOWLEDGMENT

The author thanks the project GENCOMM-NWE334 for the financial support. The project GENCOMM has been funded by the European Union with the European Regional Development Fund (ERDF) through the Interreg North-West Europe Program. The author thanks its rabbit Nelson for its valuable discussions.

References

[1] F. Azzolina-Jury, D. Bento, C. Henriques, F. Thibault-Starzyk, Journal of CO_2 Utilization 22 (2017) 97-109.

[2] V.V. Ordomsky, A.Y. Khodakov, ChemCatChem 9 (2017) 1040-1046.

[3] D. Das, G. Ravichandran, D.K. Chakrabarty, Catalysis Today 36 (1997) 285-293.

[4] M.E. Dry, Catalysis Today 71 (2002) 227-241.

[5] M.E. Dry, Applied Catalysis A: General 189 (1999) 185-190.

[6] C. Swalus, M. Jacquemin, C. Poleunis, P. Bertrand, P. Ruiz, Applied Catalysis B: Environmental 125 (2012) 41-50.

[7] A. Kim, D.P. Debecker, F. Devred, V. Dubois, C. Sanchez, C. Sassoye, Applied Catalysis B: Environmental 220 (2018) 615-625.

[8] Q. Liu, B. Bian, J. Fan, J. Yang, International Journal of Hydrogen Energy 43 (2018) 4893-4901.

[9] X. Wang, H. Shi, J. Hun Kwak, J. Szanyi, ACS Catalysis 5 (2015) 6337-6349.

[10] J-N. Park, E.W. McFarland, Journal of Catalysis 266 (2009) 92-97.

[11] W. Wang, W. Chu, N. Wang, W. Yang, C. Jiang, International Journal of Hydrogen Energy 41 (2016) 967-975.

[12] D. Wierzbicki, R. Debek, M. Motak, T. Grzybek, M.E. Gálvez, P. Da Costa, Catalysis Communications 83 (2016) 5-8.

[13] H. Takano, Y. Kirihata, K. Izumiya, N. Kumagai, H. Habazaki, K. Hashimoto, Applied Surface Science 388 (2016) 653-663.

[14] Y. Yan, Y. Dai, H. He, Y. Yu, Y. Yang, Applied Catalysis B: Environmental 196 (2016) 108-116.

[15] M.A.A. Aziz, A.A. Jalil, S. Triwahyono, R.R. Mukti, Y.H. Taufiq-Yap, M.R. Sazegar, Applied Catalysis B: Environmental 147 (2014) 359-368.

[16] R. Zhou, N. Rui, Z. Fan, C-j. Liu, International Journal of Hydrogen Energy 41 (2016) 22017-22025.

[17] G. Garbarino, D. Bellotti, P. Riani, L. Magistri, G. Busca, International Journal of Hydrogen Energy 40 (2015) 9171-9182.

[18] G. Garbarino, P. Riani, L. Magistri, G. Busca, International Journal of Hydrogen Energy 39 (2014) 11557-11565.

[19] J. Martins, N. Batai, S. Silva, S. Rafik-Clement, A. Karelovic, D.P. Debecker, A. Chaumonnot, D. Uzio, Catalysis Communications 58 (2015) 11-15.

[20] E.C. Neyts, K. Ostrikov, M.K. Sunkara, A. Bogaerts, Chemical Reviews 115 (2015) 13408-13446.

[21] E.C. Neyts, A. Bogaerts, Journal of Physics D: Applied Physics 47 (2014) 224010.

[22] F. Azzolina‐Jury, F. Thibault‐Starzyk, Topics in Catalysis 60 (2017) 1709-1721.

[23] F. Akhtar, L. Andersson, S. Ogunwumi, N. Hedin, L. Bergström, Journal of the European Ceramic Society 34 (2014) 1643-1666.

[24] T. Butterworth, R. Elder, R. Allen, Chemical Engineering Journal 293 (2016) 55-67.

[25] K. Van Laer, A. Bogaerts, Plasma Sources Science and Technology 25 (2016) 015002.

[26] K. Van Laer, A. Bogaerts, Plasma Sources Science and Technology 26 (2017) 085007.

[27] Q. Yu, M. Kong, T. Liu, J. Fei, X. Zheng, Plasma Chemistry and Plasma Processing 32 (2012) 153-163.

[28] K. Takaki, J-S. Chang, K.G. Kostov, IEEE Transactions on Dielectrics and Electrical Insulation 11 (2004) 481-490.

[29] H.L. Chen, H.M. Lee, S.H. Chen, M.B. Chang, Industrial & Engineering Chemistry Research 47 (2008) 2122-2130.

[30] T. Butterworth, R.W.K. Allen, Plasma Sources Science and Technology 26 (2017) 065008.

[31] C.-j. Liu, G.P. Vissokov, B.W.-L. Jang, Catalysis Today 72 (2002) 173-184.

[32] Z. Wang, Y. Zhang, E.C. Neyts, X. Cao, X. Zhang, B.W.-L. Jang, C-j. Liu, ACS Catalysis 8 (2018), 2093-2110.

[33] X. Liu, R.E. Truitt, Journal of the American Chemical Society 119 (1997) 9856-9860.

[34] F. Thibault-Starzyk, F. Maugé, (2012) Infrared spectroscopy. In: Che M, Védrine J (eds) Characterization of solid materials and heterogeneous catalysts: from structure to surface reactivity, pp 3-48. Wiley, New Jersey

[35] M. Digne, P. Sautet, P. Raybaud, P. Euzen, H. Toulhoat, Journal of Catalysis 211 (2002) 1-5.

[36] M. Digne, P. Sautet, P. Raybaud, P. Euzenc, H. Toulhoat, Journal of Catalysis 226 (2004) 54-68.

[37] T.A. Saleh, V.K. Gupta, Separation and purification technology 89 (2012) 245-251.

[38] S. Cassiano-Gaspar, D. Bazer-Bachi, J. Chevalier, E. Lécolier, Y. Jorand, L. Rouleau, Powder Technology 255 (2014) 74-79.

[39] R.L. Frost, J.T. Kloprogge, S.C. Russell, J. Szetu, Applied Spectroscopy, 53 (1999) 572-582.

[40] C. Lahousse, A. Aboulayt, F. Maugé, J. Bachelier, J.C. Lavalley, Journal of Molecular Catalysis, 84 (1993) 283-297.

[41] C. Lahousse, F. Maugé, J. Bachelier, J.C. Lavalley, Journal of the Chemical Society, Faraday Transactions 91 (1995) 2907-2912.

[42] J.C. Lavalley, Catalysis Today 27 (1996) 377-401.

[43] U. Janosovits, G. Ziegler, U. Scharf, A. Wokaun, Journal of Non-Crystalline Solids 210 (1997) 1-13.

[44] A.B. Kiss, G. Keresztury, L. Farkas, Spectrochimica Acta, 36A (1980) 653-658.

[45] W.B. White, R. Roy, The American mineralogist, 49 (1964) 1670-1687

[46] K.M. Parida, A.C. Pradhan, J. Das, N. Sahu, Materials Chemistry and Physics 113 (2009) 244-248.

[47] J. Sung Lee, H.S. Kim, N.K. Park, T.J. Lee, M. Kang, Chemical Engineering Journal 230 (2013) 351-360.

[48] Y.R. Zhang, E.C. Neyts, A. Bogaerts, Journal of Physical Chemistry C 120 (2016) 25923-25934.

[49] Y.R. Zhang, K. Van Laer, E.C. Neyts, A. Bogaerts, Applied Catalysis B: Environmental 185 (2016) 56-67.

[50] C. Morterra, G. Magnacca, Catalysis Today 27 (1996) 497-532.

[51] A.A. Tsyganenko, P.P. Mardilovich, Journal of the Chemical Society, Faraday Transactions 92 (1996) 4843-4852.

[52] T. Onfroy, W-C. Li, F. Schüth, H. Knözinger, Physical Chemistry Chemical Physics 11 (2009) 3671-3679.

[53] X. Krokidis, P. Raybaud, A.-E. Gobichon, B. Rebours, P. Euzen, H. Toulhoat, Journal of Physical Chemistry B 105 (2001) 5121-5130.

[54] E.C. Neyts, Plasma Chemistry and Plasma Processing 36 (2016) 185-212.

[55] P.F. Ambrico, M. Ambrico, L. Schiavulli, T. Ligonzo, V. Augelli, Applied Physics Letters 94 (2009) 051501.

[56] P.F. Ambrico, M. Ambrico, A. Colaianni, L. Schiavulli, G. Dilecce, S. De Benedictis, Journal of Physics D: Applied Physics 43 (2010) 325201.

[57] C.A. Emeis, Journal of Catalysis 141 (1993) 347-354.

[58] S. Rahmani, M. Rezaei, F. Meshkani, Journal of Industrial and Engineering Chemistry 20 (2014) 1346-1352.

[59] C. Li, Y.-W. Chen, Thermochimica Acta 256 (1995) 457-465.

[60] J. Zielinski, Journal of Catalysis 76 (1982) 157-163.

[61] C. H. Bartholomew, R.B. Pannell, Journal of Catalysis, 65 (1980) 390-401.

[62] X. Zhu, Y-p. Zhang; C-j. Liu, Catalysis Letters 118 (2007) 306-312.

[63] G. Ronchi, M. Machida Journal of Physics: Conference Series 511 (2014) 012002.

[64] K.T.A.L. Burm, · Contributions to Plasma Physics 47 (2007) 177-182.

[65] T. Butterworth, R. Elder, R. Allen, Chemical Engineering Journal 293 (2016) 55-67.

[66] M-G. Chen, A. Mihalcioiu, K. Takashima, A. Mizuno, 11th International Conference on Electrostatic Precipitation Hangzhou (2008) 681-684. Editors: Yan, Keping (Ed.).

[67] H. Wadell, The Journal of Geology 43 (1935) 250-280.

[68] E. Ozahi, M.Y. Gundogdu, M.Ö. Carpinlioglu, Advanced Powder Technology 19 (2008) 369-381.

[69] L. Li, W. Ma, Transport in Porous Media 89 (2011) 35-48.

[70] A. Rushton, A.S. Ward, R.G. Holdich, "Solid-liquid filtration and separation technology", Wiley-VCH, 2000-587 pages.

[71] A.S. Pushnov, Chemical and Petroleum Engineering 42 (2006) 14-17.

[72] H. Puliyalil, D.L. Jurkovic, V.D.B.C. Dasireddy, B. Likozar, RSC Advances 8 (2018) 27481-27508.

[73] N. Hayashi, T. Yamakawa, S. Baba, Vacuum 80 (2006) 1299-1304.

[74] L. Guo, X. Ma, Y. Xia, X. Xiang, X. Wu, Fuel 158 (2015) 843-847.

[75] Y. Li, C.-J. Liu, B. Eliasson, Y. Wang, Energy & Fuels 16 (2002) 864-870.

[76] Y. Zhang, Y. Li, Y. Wang, C.-j. Liu, B. Eliasson, Fuel Processing Technology 83 (2003) 101-109.

[77] F. Azzolina-Jury, I. Polaert, L. Estel, L.B. Pierella, Applied Catalysis A: General 453 (2013) 92-101.

[78] D.L. Jurkovic, A. Pohar, V.D.B.C. Dasireddy, B. Likozar, Chemical Engineering & Technology 40 (2017) 1-9.

Supplementary files

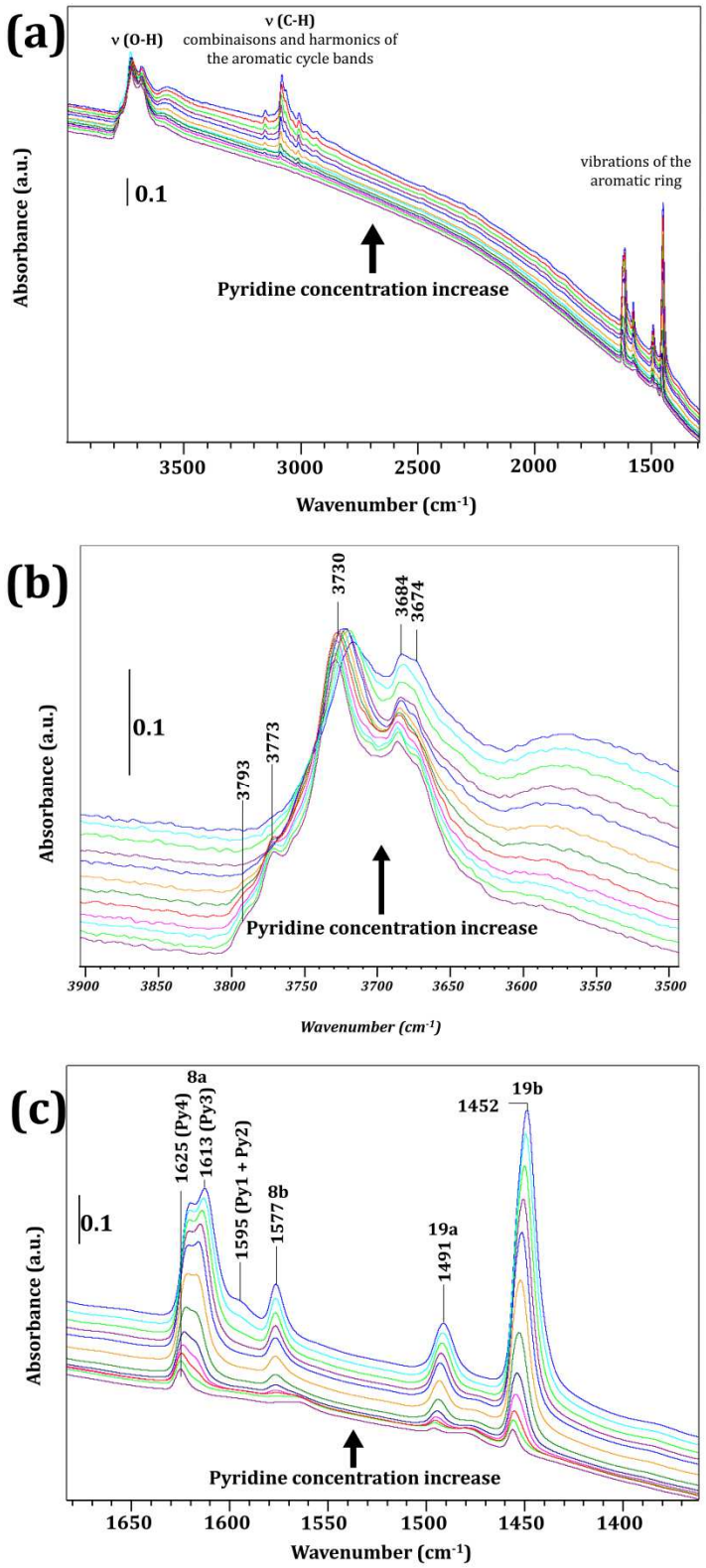

Figure S1: Pyridine adsorption spectra on nickel alumina extrudates

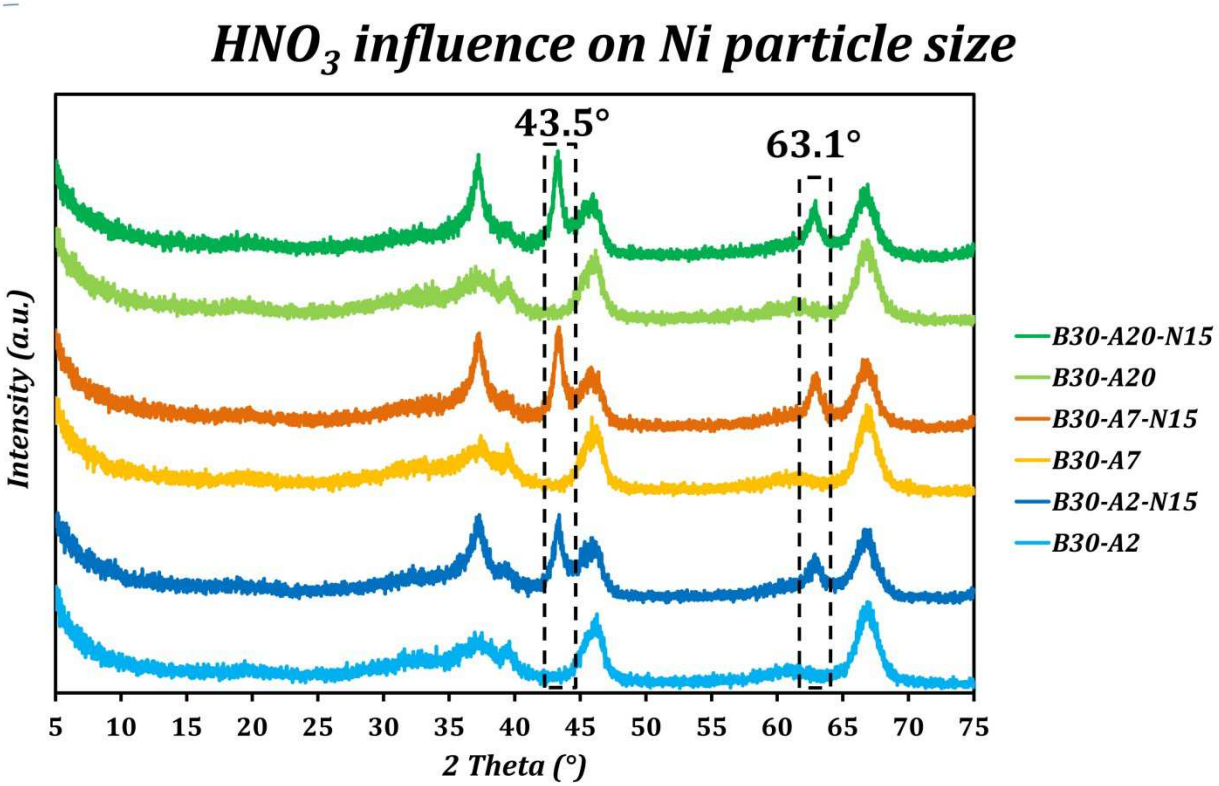

Figure S2: XRD patterns of Ni-Alumina porous extrudates

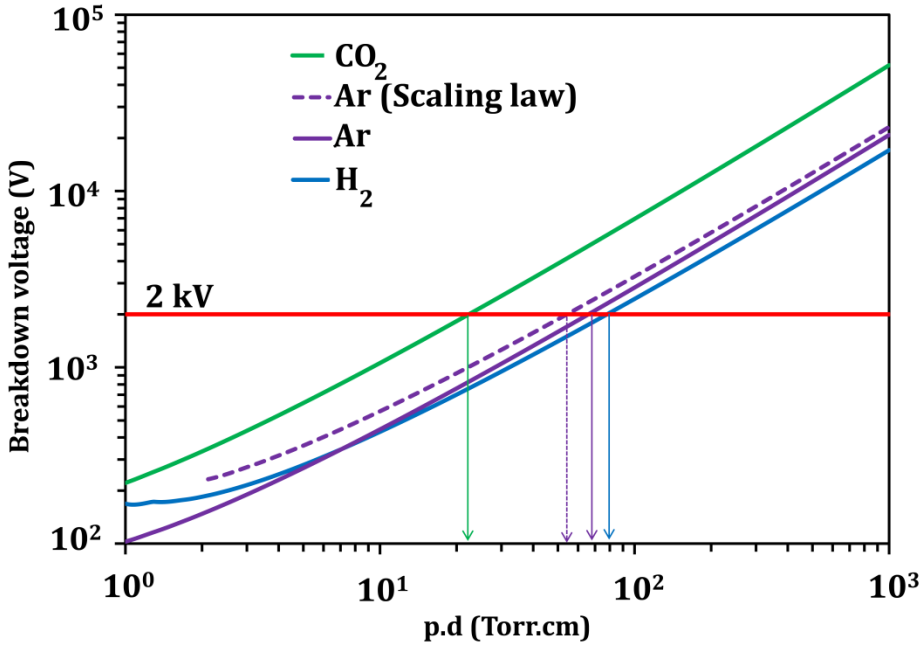

Figure S3: Critical pressure values after Paschen law and Scaling Law

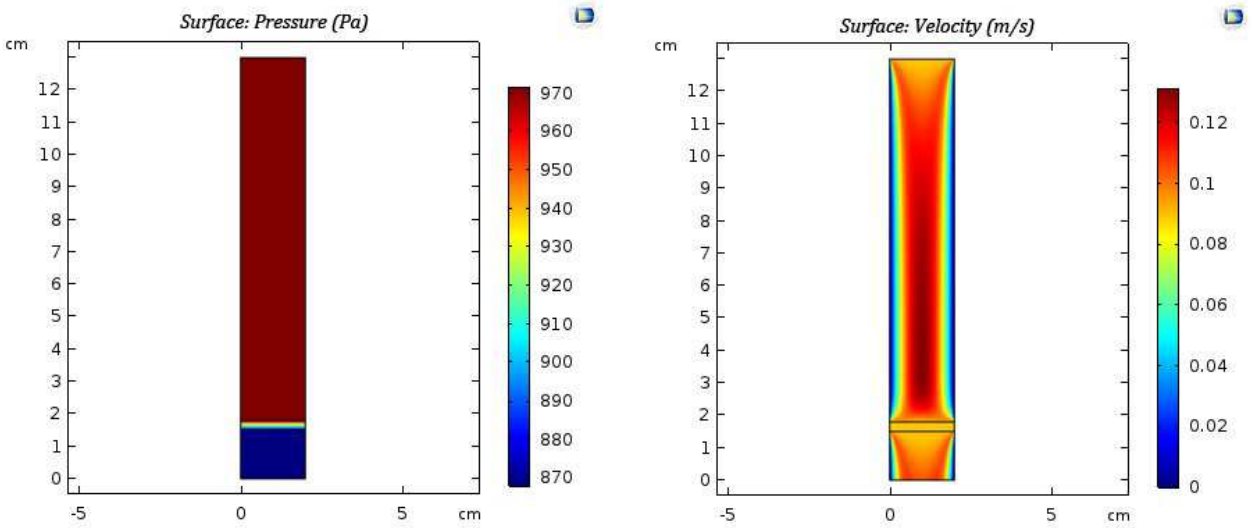

Figure S4: Velocity and pressure profiles for disc support permeability estimation at 15 mL/min STP

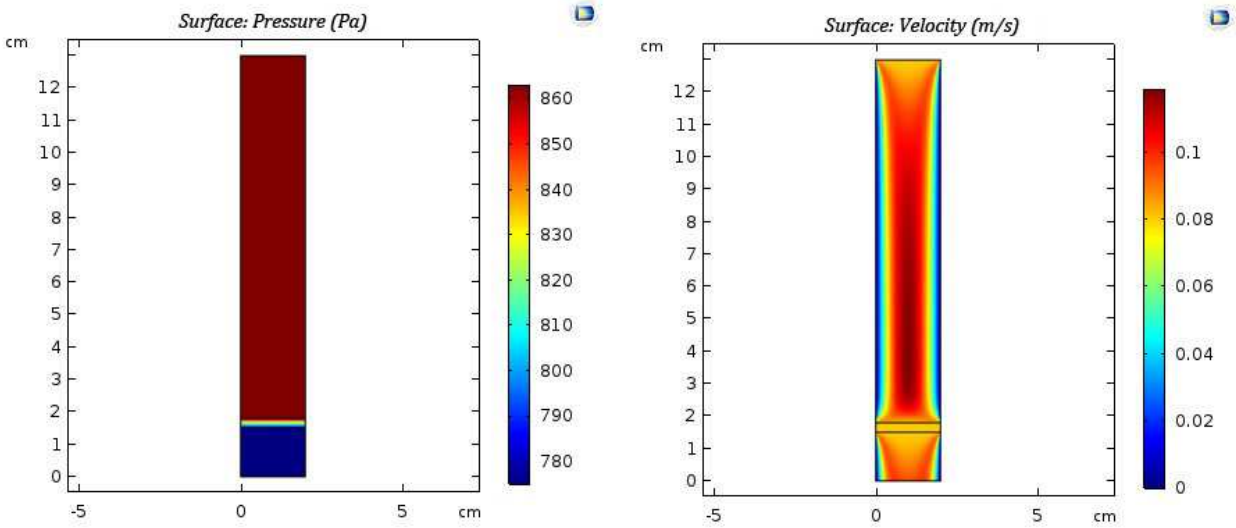

Figure S5: Velocity and pressure profiles for disc support permeability estimation at 12 mL/min STP

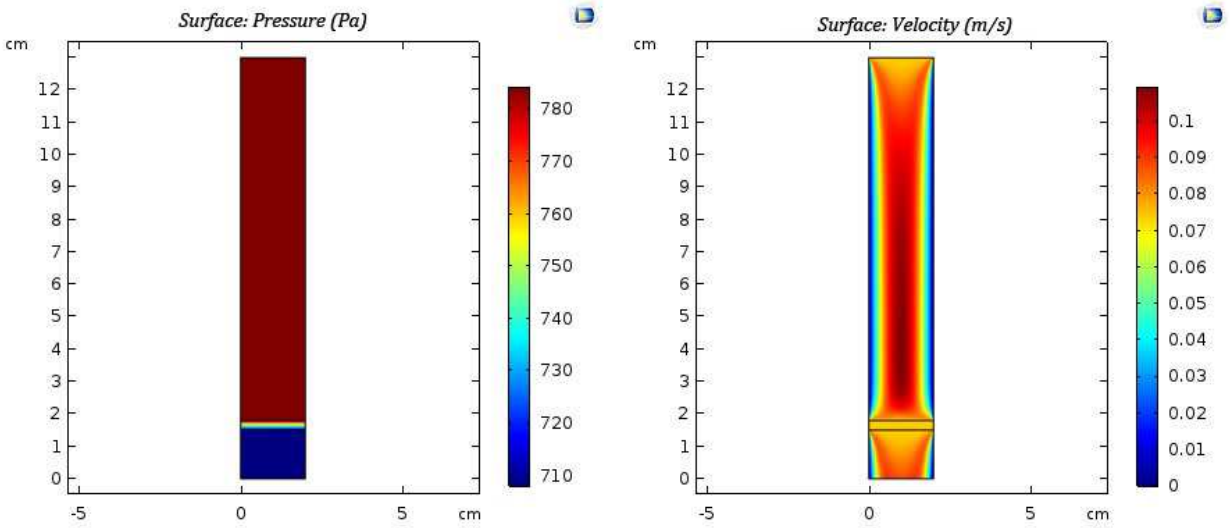

Figure S6: Velocity and pressure profiles for disc support permeability estimation at 10 mL/min STP

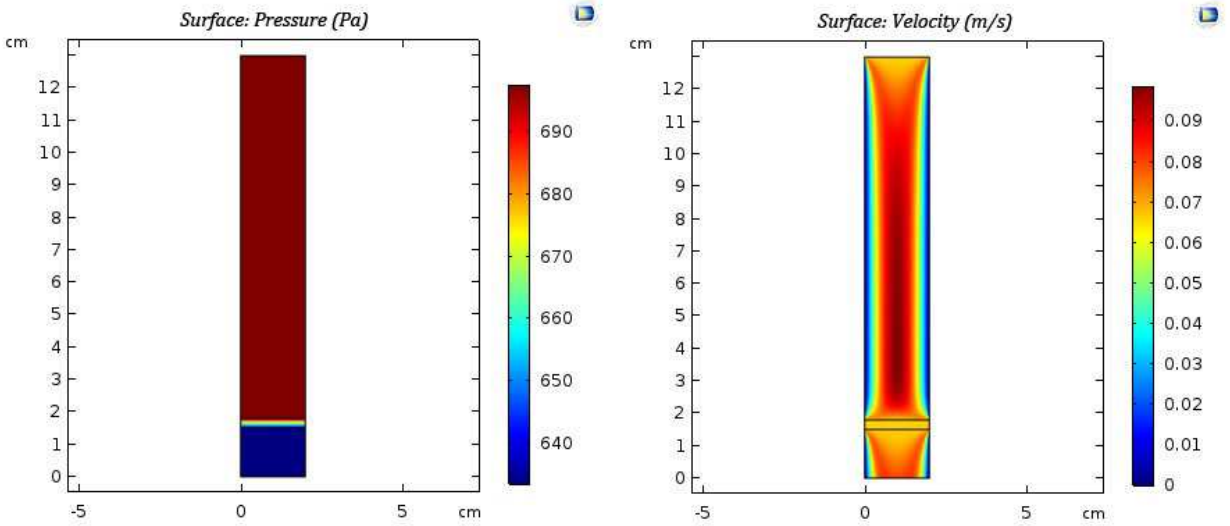

Figure S7: Velocity and pressure profiles for disc support permeability estimation at 8 mL/min STP

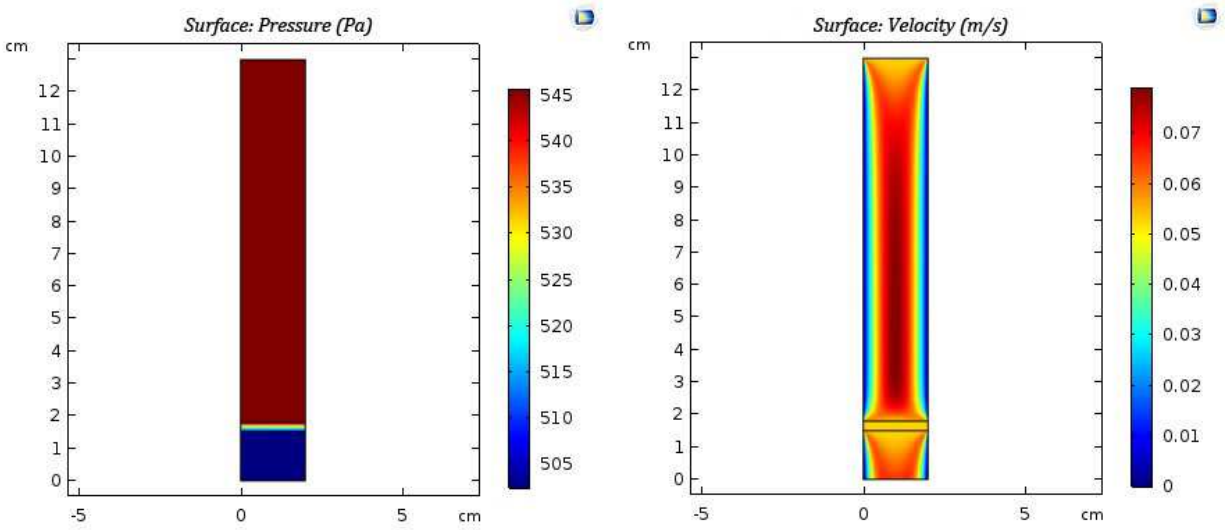

Figure S8: Velocity and pressure profiles for disc support permeability estimation at 5 mL/min STP

Supplementary table 1: Definition of catalytic parameters

Parameter	Definition
CO_2 conversion	$X_{CO_2}(\%) = \frac{F_{CO_2in} - F_{CO_2out}}{F_{CO_2in}} \times 100\%$
CH_4 selectivity	$S_{CH_4}(\%) = \frac{F_{CH_4out}}{F_{CO_2in} - F_{CO_2out}} \times 100\%$
CO selectivity	$S_{CO}(\%) = \frac{F_{COout}}{F_{CO_2in} - F_{CO_2out}} \times 100\%$
CH_4 yield	$Y_{CH_4}(\%) = \frac{F_{CH_4out}}{F_{CO_2in}} \times 100\%$
CO yield	$Y_{CO}(\%) = \frac{F_{COout}}{F_{CO_2in}} \times 100\%$

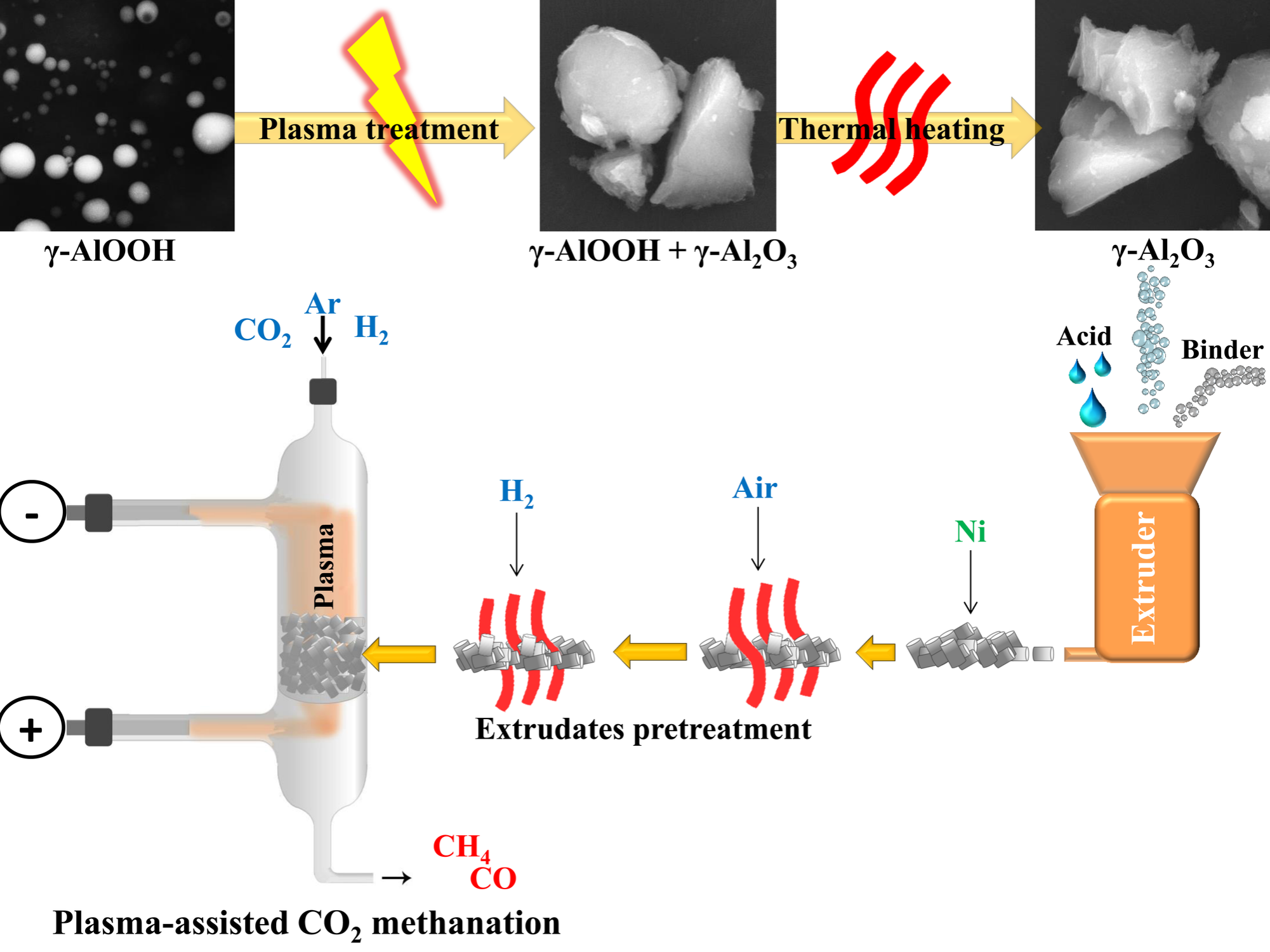
Plasma treatment
Thermal heating
γ-AlOOH
γ-AlOOH + γ-Al2O3
γ-Al2O3
Acid
Binder
Extruder
Ni
Air
H2
Extrudates pretreatment
Ar
CO2
H2
Plasma
-
+
CH4
CO
Plasma-assisted CO2 methanation